# UNIVERSITY OF EXETER

# I2 Report

Investigating the potential of actuator models for commercial wind turbine modelling and power yield prediction

**Matthew Howard**

2015
4th year MEng Group Project

I certify that all material in this thesis that is not my own work has been identified and that no material has been included for which a degree has previously been conferred on me.

Signed ......................................................

# I2 Report

## ECMM102

Title: Investigating the potential of actuator models for commercial wind turbine modelling and power yield prediction

Word count: 15,945

Number of pages: 40

Date of submission: Thursday, 28 April 2016

Student Name: Matthew Howard

Programme: MEng Mechanical Engineering

Student number: 620015740

Candidate number: 010553

Supervisor: Prof. Gavin Tabor

# Abstract

The unsteady nature of wind makes the flow over wind turbine blades extremely difficult to predict. Even with stationary inflow conditions, complex unsteady phenomena will occur. CFD simulations are a very promising method for accurately predicting the flow over the blades. Once the flow characteristics are well predicted and understood, improved and efficient engineering models can be developed for avoiding the high computational cost of complete CFD simulations. However, up to now very few CFD models of wind turbines have been validated in depth. One example of a CFD turbine model in regular use is the actuator model, which provides a method for simulating rotor flows by representing them in terms of their equivalent volume forces on the flow field. No rotor geometry is therefore included in the models and simpler forms are entirely geometry independent. This method for turbine modelling boasts a low computational expense, and therefore represents a realistic technique for industrial application.

This project formed part of a larger group investigation into the causes of wind farm power yield overestimation using current prediction techniques. Specifically focusing on the contribution of the widespread use of actuator disk models to this problem, this investigation aimed to implement and analyse a range of actuator models of increasing fidelity. This would allow the shortcomings of the commonly used, heavily simplified actuator models to be identified. The potential of more complex forms of this model variety to provide a more acceptable level of predictive accuracy and at a reasonable expense, can then be assessed. All models were implemented via modification of the standard solvers within OpenFOAM and were then compared and validated through application to two specific case studies. These models included a uniformly distributed actuator disk, a Goldstein optimally distributed disk, a blade element disk and an actuator line model. The relevant merits of each model were identified with regards to accurate power yield prediction and completeness of flow physics simulation.

Despite actuator model implementation being carried out by many parties, little research was found into the comparative fidelity of the different models. Also in many cases, little validation of the models had been carried out against real data. This provided apparent direction for the contributions of this project.

The uniformly distributed actuator disk was a poor representation of true wind turbine behaviour and is not appropriate for industrial wind farm modelling applications. The Goldstein Optimum model was proved to represent real turbines well, and was able to approximate the near rotor flow profiles almost equally to the BE approach and as a result its rotor power prediction was quite close to that of the highest fidelity ALM. The assumption of axisymmetry hindered its performance and prevented simulation of near wake effects which contribute to accurately predicting the rotor power. The use of simple actuator disk models does therefore substantially contribute to inaccuracies in wind farm power prediction as an overestimation of 0.675% was observed in this investigation.

Actuator line models were shown to provide more complete representations of true turbine dynamics and allowed the more complex near wake flow characteristics of real turbines to be simulated. This high fidelity actuator model predicted the lowest rotor power of all the

models and high confidence can be put in this approximation as a result of the model validation. Its requirement for a very fine mesh results in a large computational expense so its application to modelling of large arrays is not viable. It was concluded that actuator models in general have great potential for providing an improved solution over current wind farm predictive techniques.

# Table of Contents

# 1. Introduction

## 1.1.     *Group Project Background*

Current techniques for prediction of wind farm power yield have proven to contain inaccuracies as a discrepancy has been observed between predicted and observed power yield from wind farms. The investigation presented in this report forms a part of a larger group project to investigate the causes of these observed discrepancies and attempt to lay the foundations to reduce them through development of improved modelling techniques. The group project consists of evaluation investigations which attempt to identify the possible causes of inaccuracy in current modelling techniques, and development projects which aim to reduce the discrepancy through development of improved model functionality. The project detailed in this report is an evaluation investigation regarding the potential for use of actuator models in computational fluid dynamics (CFD) for offshore turbine simulation in industrial applications.

## 1.2.     *Individual Project Background*

Numerical techniques have proven to be a promising method for simulating the interaction of turbine rotors with the atmospheric fluid using CFD solvers. Once the flow characteristics associated with turbines are well understood, more efficient engineering models can be developed for avoiding the high computational cost of complete CFD simulations. However, up to now very few models of wind turbines have been validated in depth. One example of a CFD turbine model in regular use is the actuator model, which provides a method for simulating turbine flows by representing the rotors in terms of their equivalent volume forces on the flow field. No rotor geometry is therefore included in the models and simpler forms are entirely geometry independent. This method for turbine modelling boasts a low computational expense and high flexibility; therefore it represents one of few realistic techniques for industrial application.

Simulations of the resulting velocity deficit in the turbine wake can be used to quantify the momentum transfer, and thus the power yield of the rotor can be obtained. This method is often utilised in commercial modelling of proposed wind farms or turbine arrays, allowing the net energy gain from the site to be determined. This is pivotal in approximating the ultimate return on the investment of installing and maintaining the turbines. High levels of accuracy are required in power prediction as small discrepancies can cost millions to investors over time.

Most researchers accept that simple momentum sink zone models such as actuator disk methods are crude and make energy loss processes difficult to incorporate. However, because of their lower computational cost they are one of the few realistic approaches for gaining insight into the behaviour of substantial clusters of turbines. The versions commonly used often provide an oversimplification of the flow problem causing the more complex flow physics present in real turbine dynamics to be excluded from the simulations. Investigating the extent to which the use of these simplified actuator disk models contributes to the observed power yield

discrepancy, and also the ability of more complex varieties of actuator models to achieve more acceptable levels of accuracy, formed the main objectives of this project.

## 1.3. Project Scope and Objectives

The investigation was broken down and defined in terms of a number of deliverables. Firstly a functional actuator disk model was implemented to simulate the flowfield around a single wind turbine rotor. This acted as a datum model and represented the most simplified form of actuator model used in commercial wind farm modelling. The project then endeavoured to further develop this model in an attempt to improve on its predictive accuracy for wind turbine power yield. The resulting range of increasingly complex actuator models then included simulation of swirl in the wake, radial variances in volume forces using the 'Goldstein Optimum' distribution and coupling with blade element (BE) methods. An actuator line model (ALM) was also implemented to simulate individual rotor blade-fluid interactions and to serve as an example of the upper limit of complexity and predictive accuracy using actuator methods. Implementation of all models was carried out via modification of standard solvers provided within the open-source CFD toolbox, OpenFOAM and were based on previous implementations by a variety of external parties.

Although similar models have been implemented by a number of parties in the past, reviews of the available relevant literature has uncovered an apparent lack of comparative studies between the various models, and more importantly a lack of model validation. The main contribution of this project to the knowledge base therefore lies within the comparisons and validations carried out for the various models, and in assessment of their relative merits in commercial use. As a result the future potential of actuator models for industrial applications of individual turbine and turbine array simulations can be determined.

## 1.4. Case Studies

Two specific case studies were used in this investigation. Firstly, a theoretical 5MW offshore wind turbine was defined by the National Renewable Energy Laboratory to serve as a reference case for analysis of turbine models. Enough information about the rotor geometry was provided such that the turbine could be simulated using a wide variety of CFD models. Since the project in general is concerned primarily with offshore wind turbine arrays, this provided an ideal case for model comparison as well as to assess the performance of each model when used in a typical commercial case. Each of the actuator models was set up to simulate the transient behaviour of this specific turbine. The operating conditions for the turbine were kept constant, as were the simulation variables including mesh density, turbulence models and model coefficients. The resulting predictions of each model were then compared to highlight any differences that their varying complexity may have on their calculation of turbine flow behaviour and primarily their resulting power yield approximation.

A second case study served as validation of the model predictions through direct comparison to experimental observations of true wind turbine behaviour. The large scale wind

tunnel experimentation known as 'Model rotor EXperiments In COntrolled conditions' or MEXICO experiments was carried out in 2007 by ECN Wind Energy Technology, Netherlands. This undertaking produced an extensive collection of experimental data regarding the flow dynamics and operation of a 5m diameter wind turbine known as the MEXICO rotor. The wind tunnel case was simulated using the actuator line model previously implemented and the resulting velocity profiles predicted by the model were directly compared to those observed in the MEXICO experiments. This allowed the accuracy of the most complex form of actuator model implemented within this project to be evaluated, and the potential for actuator models as an adequate predictive method for wind farms to be quantified.

## 1.5. Assumptions, Limitations and Project Links

In order to focus the outcomes of the investigation and avoid the model variances becoming clouded by other external fluctuations, it was decided to limit the investigation to certain simplified cases. For example, only uniform inlet conditions were used in the simulations. As such, atmospheric boundary layer (ABL) effects are neglected and the turbines receive a steady and consistent influx. Another aspect of the group project carried out by Hyde-Linaker, G. investigates the importance of ABL inclusion in turbine simulations.

The investigation was also limited to turbines with zero yaw, such that the rotor plane is perpendicular to the direction of flow. March, T. carried out further investigations within the group regarding the use of simple actuator disks to model yawed turbine flow.

Finally, due to time constraints on model implementation, cases in this investigation are set up using a prescribed rotational speed for each turbine, this is not representative of real turbines where their rotational speed is dependent on the inflow conditions interacting with the rotor geometry. A project within the group by Ashby, B. aimed to develop a simple actuator disk model where the rotational speed of each turbine is determined by sampling of the upstream flow conditions. With this it is clear that the assumptions and limitations of this investigation are considered and accounted for by other members of the group and in this way the projects are linked in their ultimate objectives.

# 2. Literature Review

## 2.1. Actuator Model Background

### 2.1.1. Rankine-Froude Actuator Disks (Momentum Theory)

The use of actuator disks to represent wind turbine flow problems was a technique first developed by [1]Froude (1889), in an extension of the work carried out by [2]Rankine (1865) on momentum theory relating to rotor energy balancing equations. This one dimensional analytical model presented an idealized representation of turbine energy transfer. The model was later analysed by [3]Betz (1920), who used the principles of conservation of mass and momentum of the fluid passing through the actuator disk region to quantify a theoretical maximum energy

extraction by the turbine. This bounding quantity known as the Betz limit, was equal to 16/27 or 59.3% of the incoming kinetic energy. The simplifications and assumptions made by this model result in its inability to account for the complex flow dynamics present in real cases. In particular it excludes radial force distributions and addition of angular momentum to the flow in the wakes and as a result is incapable of accurately modelling wake interactions when multiple turbines operate in close proximity.

### 2.1.2. **Blade Element Momentum Theory**

[4]Glauert (1963) later brought major development to this limited theory by enhancing the models ability to account for radial parameter distributions, thus extending the model to a three dimensional analysis. Essentially the model applies momentum balance equations for individual annular stream tubes which sum to describe the energy transfer more accurately over the actuator disk region. Where the Rankine-Froude model assumed a uniform loading and velocity over the disk, Glauert provided the ability for the model to account for more realistic radial variations.

### 2.1.3. **Generalised Actuator Disk Model**

The generalised actuator disk method used for rotor flow problems is essentially an inviscid extension of the BEM theory. Here, the permeable actuator disk is placed in the flow domain and is set to impart volume forces on the fluid flow that represent the momentum extraction and also impart swirl in the wakes. Axisymmetric versions of the method have been developed and solved either by analytical or semi-analytical methods such as by [5]Wu (1962), [6]Hough and Ordway (1965), [7]Greenberg (1972), and [8]Conway (1995), or by finite difference/volume methods for example by [9,10,11]Sorensen et al. (1992) and [12]Madsen (1996). Also by finite element methods (FEM), as formulated by [13]Masson et al. (2001) who solve the unsteady 3D flowfield around a HAWT. These facilitate natural unsteady wake development, but the semi-analytical methods are generally solved as steady state problems. The magnitudes of the volume forces relative to the incoming fluid flow characteristics are generally calculated analytically. The complexity of these models is determined by the methods used to define the volume force distributions across the actuator region. The simplest models such as those implemented by [14]Javaheri (2013) to compare turbulence models in actuator disk methods, use a uniform distribution similar to the Froude-Rankine analytical model. More realistic radial distributions can be implemented such as in the models developed by [15]Svenning (2010) and [16]Mikkelson (2001).

### 2.1.4. **Addition of Blade Element Method**

Coupling of the blade element method with actuator disks allows the resulting flowfield volume forces to become dependent on the rotor geometry, unlike in simpler actuator disk methods which are completely independent of rotor geometry. The mathematical process was originally developed by Froude but the method has been recently introduced into numerical

actuator disk solutions which are capable of discretizing the disk much more finely than in an analytical solution. Implementation of look-up tables for experimentally characterised aerofoils into the solver allows blade forces to be calculated for each cell depending on its radial location within the actuator disk. This method was utilised by [17]Jeromin et al. (2014) to develop an actuator disk model for the MEXICO rotor within OpenFOAM. His results were validated against experimental data and were shown to provide a good representation.

### 2.1.5. **Actuator Line Model**

The assumption of axial symmetry of the models can be removed and dynamic forces along the lengths of the individual turbine blades can be modelled through the application of actuator line models; a concept introduced more recently by [18]Sorensen and Shen (2002). This method represents the individual rotor blades by their equivalent volume forces distributed along lines through the domain, radiating from a central point. Blade element look-up tables are used to define the force distributions along these lines. The SOWFA project carried out by the [19]National Renewable Energy Laboratory (2013) compiled a set of high fidelity wind farm solvers that used transient actuator line methods coupled with inlet conditions from a precursor atmospheric boundary layer, large eddy simulation (LES). The methods implemented here will provide useful resource when implementing high fidelity actuator line models and also when coupling these models to LES.

## 2.2. *Resulting Project Contributions*

Due to the apparent lack of investigations regarding model accuracy comparisons in the pre-existing literature, the project will evaluate the limits of the various model's fidelity and their relative merits for power yield prediction will be assessed. The trade off between model accuracy and expense imposes a requirement to determine whether the highest accuracy forms of actuator disk models are significant improvements over the simpler, commonly used, cheaper modelling techniques. In the end, the project aims to investigate whether the commonly used, simplified actuator disk methods are responsible for contributing the power discrepancy. Also the potential of high fidelity actuator models for reducing the power yield discrepancy, while remaining suitable for industrial application must be investigated. This is the main contribution that this project will endeavour to make.

## 2.3. *Methodology Sources*

### 2.3.1. **Actuator Model Implementation**

[15]Svenning (2010) has described a simple way to define actuator disk regions in modified OpenFOAM solvers. This involves a method of looping over the cells in a given domain to identify those that lie within a geometrically predefined actuator region as well as their radial position from a reference location (at the centre of the actuator region). A new volume force

field is also defined in his technique to be computed as part of the numerical solution, this term is also included in the governing velocity equation allowing it to influence the flow momentum.

As previously discussed [15]Svenning (2010) implemented a simple actuator disk model in OpenFOAM. This involved distribution of thrust and torque forces across a permeable disk representing the rotor swept area. These axial and tangential volume forces are responsible for simulating a wake and imparting swirl in the wake respectively. In his report, Svenning appended his code used to realize this model through modification of the standard simpleFoam solver. This was implemented and proved to be fairly unambiguous, allowing it to be used as a basis to build more complex actuator disk variations upon. The code, which was originally prepared only for steady-state, RANS based simulations, was modified to work in pisoFoam such that transient large eddy simulations (LES) of turbine behaviour could be carried out.

Finally, the [19]NREL (2013) provided a comprehensive technique for development of high fidelity actuator line methods. The techniques suggested were implemented in pisoFoam to form the highest complexity form of actuator model used within this investigation. This technique also contained a method for coupling of blade element look-up tables and so Svenning's model was also modified to include this functionality. This would create an actuator disk with blade element coupling. Four actuator models of increasing complexity were developed and analysed within the investigation; a uniformly distributed actuator disk, a prescribed radially distributed actuator disk, a blade element coupled actuator disk and also a blade element actuator line model.

### 2.3.2. **Power Yield Prediction**

The principal use of CFD analysis in modelling of wind farm arrays is the prediction of the power output from a proposed wind farm site. The power output, being the primary objective of the wind farm system itself, is approximated before construction of the wind farm to evaluate the financial gain through energy generation versus the expense of construction, maintenance etc of the turbines. As such, modelling techniques must be capable of providing an acceptable level of accuracy in their approximation of turbine power output. The values of power output obtained by all implemented forms of actuator models for a given set of controlled conditions should be compared. This allows the effect that increased modelling fidelity has on the predictive accuracy of the models in terms of power to be observed.

Since actuator models often do not directly include the effects of the generator systems, gearing systems and control systems, the true electrical power output obtained from a turbine cannot be approximated directly in the CFD. Instead, the rotor power can be computed, which represents the mechanical power of the rotor that is available for conversion to electrical energy by the generator. This rotor power, gained from the extraction of energy from the flow is related to the forces experienced by the rotor as it interacts with the fluid flow.

Avoiding modelling the blade motions through actuator techniques means that pressure integration over the blade surface cannot be used to directly estimate the mechanical power transferred to the machine from the flow. Consequently, published research on simplified descriptions of turbines of all kinds has focussed instead upon calculating the energy lost from

the flow. [20]Gebreslassie et al. (2015) used this method to approximate power from an array of interacting tidal turbines. A similar approach has been undertaken in the work presented here. The theory behind this method of rotor power prediction is described in section 3.4.1.

## *2.4. Case Study Literature*

### 2.4.1. **NREL 5 MW Reference Turbine**

In order to compare the various forms of actuator models it is necessary to define a comparison case. Since this investigation is generally concerned with modelling techniques applied to large offshore wind turbines, the chosen case involved a full-scale offshore turbine geometry described by the [21]National Renewable Energy Laboratory (2009). This theoretical turbine design was developed to serve as a realistic and standardized input for the analysis of offshore wind predictive technologies. As a result the detailed specification of a large wind turbine that is representative of typical utility-scale land and sea-based multi-megawatt turbines was established. The resulting gross properties of the turbine are defined as in Table 1.

Table 1. Gross properties of the NREL offshore turbine

| Rating | 5 MW |
|---|---|
| **Rotor Orientation, Configuration** | Upwind, 3 blades |
| **Control** | Variable Speed, Collective Pitch |
| **Drivetrain** | High Speed, Multiple-Stage Gearbox |
| **Rotor, Hub Diameter** | 126 m, 3 m |
| **Hub Height** | 90 m |
| **Cut-In, Rated, Cut-Out Wind Speed** | 3 m/s, 11.4 m/s, 25 m/s |
| **Cut-In, Rated Rotor Speed** | 6.9 rpm, 12.1 rpm |
| **Rated Tip Speed** | 80 m/s |
| **Overhang, Shaft Tilt, Precone** | 5 m, $5^0$, $2.5^0$ |
| **Rotor, Nacelle, Tower Mass** | 110,000 kg, 240,000 kg, 347,460 kg |

The turbine rotor consisted of six separate aerofoil sections as well as two cylindrical sections at the blade root. These included a National Advisory Committee for Aeronautics (NACA) based aerofoil defined as NACA64_A17 and a number of Delft University developed aerofoils defined as DU21_A17, DU25_A17, DU30_A17, DU35_A17 and DU40_A17. These were distributed along the span of the blade as in Table 2.

Table 2. NREL offshore turbine blade geometry definition.

| Node | Radial Node (m) | Twist ($^0$) | Chord (m) | Aerofoil |
|---|---|---|---|---|
| 1 | 2.8667 | 13.308 | 3.542 | Cylinder 1 |
| 2 | 5.6000 | 13.308 | 2.854 | Cylinder 1 |
| 3 | 8.3333 | 13.308 | 4.167 | Cylinder 2 |
| 4 | 11.7500 | 13.308 | 4.557 | DU40_A17 |
| 5 | 15.8500 | 11.480 | 4.652 | DU35_A17 |
| 6 | 19.9500 | 10.162 | 4.458 | DU35_A17 |

| 7 | 24.0500 | 9.011 | 4.249 | DU30_A17 |
|---|---------|-------|-------|----------|
| 8 | 28.1500 | 7.795 | 4.007 | DU25_A17 |
| 9 | 32.2500 | 6.544 | 3.748 | DU25_A17 |
| 10 | 36.3500 | 5.361 | 3.502 | DU21_A17 |
| 11 | 40.4500 | 4.188 | 3.256 | DU21_A17 |
| 12 | 44.5500 | 3.125 | 3.010 | NACA64_A17 |
| 13 | 48.6500 | 2.319 | 2.764 | NACA64_A17 |
| 14 | 52.7500 | 1.526 | 2.518 | NACA64_A17 |
| 15 | 56.1667 | 0.863 | 2.313 | NACA64_A17 |
| 16 | 58.9000 | 0.370 | 2.086 | NACA64_A17 |
| 17 | 61.6333 | 0.106 | 1.419 | NACA64_A17 |

This information was implemented into the case set-up in as much detail as is allowed by the individual models. The simpler models which are geometry independent could only utilise the rotor size and analytically obtained total volume forces, whereas the complex blade element models can include the entire rotor span parameter distributions.

### 2.4.2. MEXICO Experiments

The [22]Model rotor Experiments in Controlled Conditions (2006) or MEXICO project was a measurement campaign that involved the extensive measuring of load, pressure and flow data from a 3 bladed wind turbine. The LLF (Large LowSpeed Facility) of the German-Dutch Wind tunnel DNW, which has an open section of 9.5m x 9.5m was used to provide a uniform inlet with several flow conditions, including 2 different rotational speeds (324 rpm and 424 rpm), several wind speeds (ranging from 10 to 30 m/s), several pitch angles (from -5.3 deg to 1.7 deg) and several yaw-inflow angles (from 0 deg to 45 deg).

The wind turbine has a rotor diameter of 4.5 m. The blades rotate in a clockwise direction and are twisted and tapered. Their design is based on 3 different aerodynamic profiles: DU91- W2-250, RISO-A1-21 and NACA 64-418 and together they have become known as the MEXICO rotor. These aerofoils are distributed along the blade span as in Table 3.

Table 3. MEXICO rotor blade geometry definition.

| Node | Radial Node (m) | Twist (⁰) | Chord (m) | Aerofoil |
|------|-----------------|-----------|-----------|----------|
| 1 | 0.39972 | 0.000 | 0.195 | Cylinder1 |
| 2 | 0.41808 | 0.000 | 0.195 | Cylinder1 |
| 3 | 0.42216 | 0.000 | 0.090 | Cylinder1 |
| 4 | 0.48132 | 0.000 | 0.090 | Cylinder1 |
| 5 | 0.54864 | 8.200 | 0.165 | DU91_W2_250 |
| 6 | 0.61800 | 16.400 | 0.240 | DU91_W2_250 |
| 7 | 0.82200 | 12.100 | 0.207 | DU91_W2_250 |
| 8 | 1.02600 | 8.300 | 0.178 | DU91_W2_250 |
| 9 | 1.13820 | 7.100 | 0.166 | DU91_W2_250 |
| 10 | 1.23000 | 6.100 | 0.158 | RISOA1_21 |
| 11 | 1.31967 | 5.500 | 0.150 | RISOA1_21 |
| 12 | 1.43400 | 4.800 | 0.142 | RISOA1_21 |
| 13 | 1.54620 | 4.000 | 0.134 | RISOA1_21 |
| 14 | 1.63800 | 3.700 | 0.129 | NACA64_418 |
| 15 | 1.72776 | 3.200 | 0.123 | NACA64_418 |

| 16 | 1.84200 | 2.600 | 0.116 | NACA64_418 |
|----|---------|-------|-------|------------|
| 17 | 2.04600 | 1.500 | 0.102 | NACA64_418 |
| 18 | 2.17248 | 0.700 | 0.092 | NACA64_418 |
| 19 | 2.19696 | 0.469 | 0.082 | NACA64_418 |
| 20 | 2.23348 | 0.231 | 0.056 | NACA64_418 |
| 21 | 2.25000 | 0.000 | 0.011 | NACA64_418 |

Flow data was obtained via the use of Particle Image Velocimetry (PIV) measurements which were performed along multiple PIV windows upstream and downstream of the turbine. Two radial and two axial traverses were performed.

The MEXICO rotor is a thoroughly investigated blade geometry and so will be the basis for experimental validation of geometry dependent models due its plentiful sources of comparative data. In this work three different wind speeds have been considered (10 m/s, 15 m/s and 24 m/s), while the rotational speed has been kept constant at 424.4 rpm and a blade pitch of -1.3⁰. These conditions correspond to pre-stall, design conditions and post-stall respectively. The PIV data will provide three components of velocity measurements within the near wake region and slightly upstream of the turbine. As a result it is expected that only the actuator line based models will be able to accurately predict the flow velocities in these regions.

# 3. Theoretical Background, Model Implementation and Data Processing

## 3.1. Fundamental Actuator Theory

### 3.1.1. Actuator Disk (Momentum) Theory

The one dimensional analysis of wind turbine flow problems initially developed by Froude and Rankine provides the basis for all actuator representations of turbine rotors. The problem is simplified such that only the overall momentum transfer across the rotor's swept area is considered. The theory is presented here as a basis to be built upon by the more complex models that follow.

The actuator disk theory replaces the turbine rotor swept area with a permeable disk of equivalent area across which the rotor blade forces are distributed. These forces alter the fluid flowfield around the disk, governed by mass conservation and momentum balance equations. The theory operates under many assumptions including a lack of viscous effects such as frictional drag or momentum diffusion; a homogenous, incompressible, steady state fluid flow; a constant thrust per unit area over the disk; continuity of velocity through the disk and axial symmetry resulting in an infinite number of blades.

The incoming free-stream fluid flows with a velocity $U_\infty$ at a static pressure $p_0$. Analysis of this scenario using actuator disk theory applies a control volume bounded by the surface walls of the stream tube plus inlet and outlet boundaries as shown in Fig.1. The fluid flow parameters are then quantified at four locations; L1 – free-stream location at the inlet, L2 – upstream of the rotor, L3 – downstream of the rotor, L4 – far wake region at the outlet.
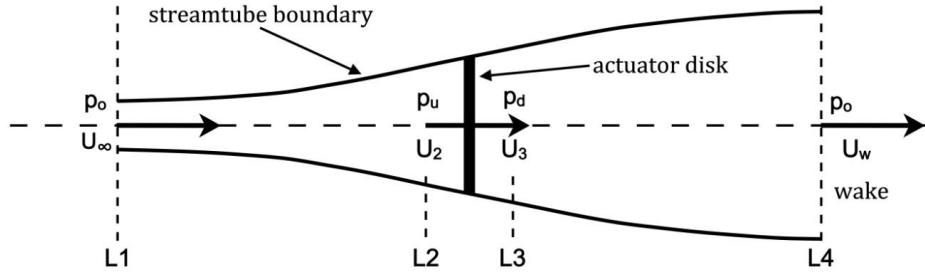
Fig.1 Flowfield through an actuator disk

The mass flow rate must remain constant throughout the control volume, making the continuity equation along the stream tube as written in Eq.1.1.

$$\rho A_\infty U_\infty = \rho A_d U_d = \rho A_w U_w \qquad \text{Eq. 1.1}$$

The assumption of continuity of velocity through the disk also shows that the velocity before the disk $U_2$ and after the disk $U_3$ should be equal, and both should be equal to the velocity at the disk $U_R$. The mass flow rate is therefore given by Eq.1.2.

$$\dot{m} = \rho A U_R \qquad \text{Eq. 1.2}$$

The conservation of linear momentum equation can then be applied on either side of the actuator disk to obtain the thrust force T via Eq.1.3.

$$T = \dot{m}(U_\infty - U_w) \qquad \text{Eq. 1.3}$$

Due to the assumption of frictionless flow, no work or energy transfer is done. Bernoulli principles can then be applied across the rotor. Applying energy conservation using Bernoulli's equation between locations 1 and 2, then 3 and 4 and combining the two subsequent equations, the pressure decrease $\Delta p$ across the control volume can be defined by Eq.1.4.

$$\Delta p = \frac{1}{2}\rho(U_\infty^2 - U_w^2) \qquad \text{Eq. 1.4}$$

Also the thrust on the actuator disk rotor can be expressed by Eq.1.5 as the sum of the forces on each side as a result of the pressure difference, $p_u - p_d$.

$$T = A\Delta p = \frac{1}{2}A\rho(U_\infty^2 - U_w^2) \qquad \text{Eq. 1.5}$$

The power output of the rotor is also required to predict the yield from the turbine using this model. This power is related to the thrust force and the velocity through the rotor by Eq.1.6.

$$P = TU_R = \frac{1}{2}A\rho(U_\infty^2 - U_w^2)U_R \qquad \text{Eq. 1.6}$$

This power is usually defined in terms of the axial induction factor $\alpha$ given by the ratio of the flow velocity decrease between the inlet and rotor to the free-stream flow velocity. The power is therefore given by Eq.1.7.

$$P = 2\rho A\alpha U_\infty^3(1 - \alpha)^2 \qquad \text{Eq. 1.7}$$

The performance parameters of turbine rotors including power coefficient $C_P$, thrust coefficent $C_T$, and the tip-speed ratio λ are expressed in dimensionless form in Eq. 1.8, 1.9 and 1.10 respectively.

$$C_P = \frac{2P}{\rho U_\infty^3 \pi R^2} \quad \text{Eq. 1.8} \qquad C_T = \frac{2T}{\rho U_\infty^2 \pi R^2} \quad \text{Eq. 1.9} \qquad \lambda = \frac{R\Omega}{U_\infty} \quad \text{Eq. 1.10}$$

### 3.1.2. **Annular Stream Tube (BEM) Theory**

Unlike Rankine-Froude actuator disks, real turbine rotors never have uniform force distributions. In an attempt to include radial variations in rotor loading, the flowfield through the actuator disk is divided into a number of radially independent annular streamtubes in Glauert's blade element momentum method. The radial independence of the streamtubes along with a lack of pressure forces on the control volume and axisymmetric flow, represent the main assumptions of this classical theory.

The conservation of linear momentum allows Eq.1.3 for the Thrust and Eq.1.6 for the extracted power to be applied for each of the annular streamtube elements, the balance of axial and angular momentum for each annular element is given by Eq.2.1 and 2.2 respectively.

$$\Delta T = 2W_z \Delta \dot{m} \quad \text{Eq. 2.1} \qquad \Delta Q = 2W_\theta r \Delta \dot{m} \quad \text{Eq. 2.2}$$

Where $\Delta \dot{m} = \rho(U_\infty - W_z)\Delta A$ and $\Delta Q$ is the resulting torque on each blade element. The induced velocity $W_z = U_\infty - u$ and angular velocity $W_\theta$. Although $W_\theta$ is zero in front of the disk, the angular velocity on the disk is equal to $-W_\theta$, and just after the disk $-2W_\theta$. In the wake the angular velocity is preserved along each streamsurface as $rW_\theta = r_s W_{\theta s}$ where $r_s$ is the stream-surface radial distance.

## *3.2.* *Theory and Implementation of Actuator Models in CFD*

Implementation of actuator disks in CFD is known as the generalised method. This is one of the mostly widely implemented industrial tools for wind farm simulation due to its relative accuracy and low computational cost. The models can vary greatly in complexity and also in accuracy. The simplest models apply only a pressure drop to the fluid as it passes through the disk region whereas the most complex are able to simulate bound root and tip vortices.

In order to make use of the various turbine models, a CFD solver is used. The OpenFOAM package is a set of C++ libraries designed for solving partial differential equations. The turbine models were implemented as C++ classes called upon by the solver. A finite volume approach is then used to discretize the governing equations for which solutions are obtained iteratively for an array of discrete points representing the flow domain.

### 3.2.1. **Defining an Actuator Region**

Svenning described a method for defining an actuator region across which an array of body force field values could be distributed. This method can be applied to a range of OpenFOAM standard solvers and involved:

- Addition of an extra source term in the U-equation

     UEqn () == - fvc :: grad (p ) + VolumeForce
- Addition of an actuator class, which is capable of: Reading the defined actuator geometry. Finding all cells located within the actuator region. Identifying each cell's radial position. Adding a volume force to each of these cells according to some prescribed equation or rule.

### 3.2.2. Ranking-Froude 1D Actuator Disk

The prescribed equation used to define the distribution of volume forces over the actuator region can range in complexity. The simplest solution is to create a Rankine-Froude disk where the volume force does not vary with radial distance from the centre of rotation for the represented turbine. This involves uniformly distributing the required total thrust forces over the actuator region.

This can be achieved by simply quantifying the total number of radial cell centres within the actuator region and giving each discrete location an equal share of the total thrust. It is also possible to add a torque force and distribute this in a similar manner to include simulation of wake swirl effects. Since this model is intended to represent a Rankine-Froude actuator disk, only the momentum changes across the actuator region are considered.

### 3.2.3. Goldstein Optimum Model

The model developed by Svenning represents a slightly more complex Actuator Disk model as it reduces the fluid momentum passing through an annular cylinder by application of a thrust force T, and imparts swirl in the wake via application of a torque force Q. These volume forces are varied radially in accordance with [22]Goldstein's (1929) Optimum distribution, giving the forces in the form of Eq.3.1 and 3.2 where $R_H$ is the interior radius of the annular disk and $R_P$ is the exterior radius.

$$f_{bx} = A_x r^* \sqrt{1 - r^*} \;\; \text{Eq. 3.1} \qquad f_{b\theta} = A_\theta \frac{r^* \sqrt{1 - r^*}}{r^*(1 - r_h') + r_h'} \;\; \text{Eq. 3.2} \qquad \text{where,} \;\; r^* = \frac{(r/R_P) - r_h'}{1 - r_h'}$$

The total prescribed thrust T and torque Q provide the limit of the summation of the volume force distributions and so provide a means to calculate the axial and tangential constants, $A_x$ and $A_\theta$ respectively via Eq.3.3 and 3.4.

$$A_x = \frac{105}{8} \frac{T}{\pi \Delta (3R_H + 4R_P)(R_P - R_H)} \qquad \text{Eq. 3.3}$$

$$A_\theta = \frac{105}{8} \frac{Q}{\pi \Delta R_P (3R_P + 4R_H)(R_P - R_H)} \qquad \text{Eq. 3.4}$$

The Goldstein optimum distribution used in this actuator disk model is derived as the force distribution that results in a minimum induced loss, thereby maximising efficiency. A turbine that is optimally distributed in this way therefore represents an ideal turbine operating

at the Betz limit. This distribution is often used in the design of efficient propellers and turbine rotors. The collective code used to implement this model can be found in [15]Svenning (2010).

### 3.2.4. **Blade Element Model**

To include the effects of rotor geometry characteristics, i.e. the specific aerofoils that constitute the rotor blades, blade element theory needs to be added to the actuator disk. Essentially, a virtual blade is inserted into the actuator region and is divided into a number of sections. The flow at each section will vary since each of the blade elements has a different relative speed and aerofoil geometry. Numerical integration over the blade span determines the flow over the entire blade. The method operates under some assumptions; mainly that the forces on the blade elements are solely the result of the lift and drag coefficients for that section and the individual blade elements do not interact aerodynamically with one another.

Data tables for lift and drag coefficients are available for a number of aerofoils from conducted wind tunnel experiments, where the relative fluid velocity over the stationary aerofoil is used to characterise its body-force characteristics. A cross section of a standard HAWT rotor blade geometry is presented in Fig.2.
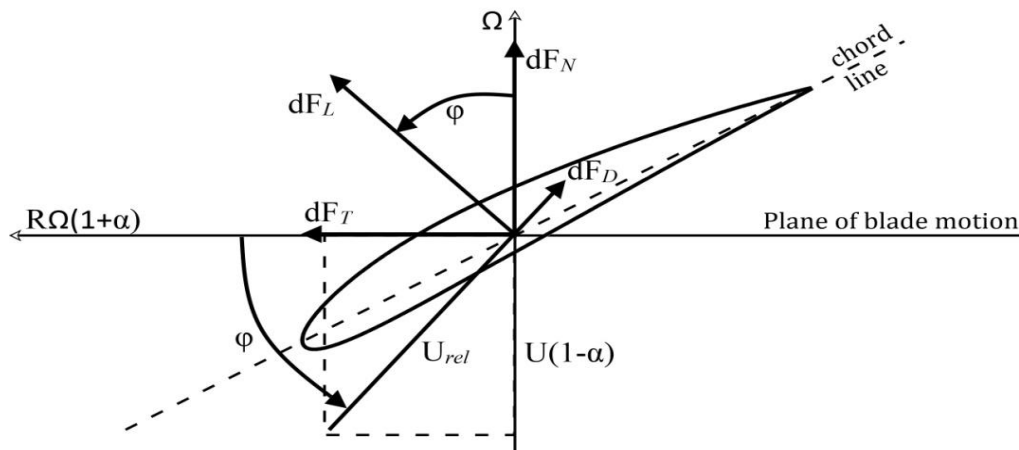


Fig.2 – Velocity and force vectors on a rotor blade cross-section

From this, the local velocity relative the blade is given by Eq.4.1, and its angle to the rotor plane can be defined by Eq.4.2.

$$U_{rel} = \frac{U_\infty(1-a)}{\sin\varphi} \quad \text{Eq. 4.1} \qquad \tan\varphi = \frac{U_\infty(1-a)}{\Omega r(1+a')} = \frac{(1-a)}{(1+a')\lambda_r} \quad \text{Eq. 4.2}$$

Equations for the lift and drag forces can then be derived via rigid-body dynamics to produce Eq.4.3 and 4.4 respectively.

$$dF_L = C_L \frac{1}{2}\rho U_{rel}^2 c dr \quad \text{Eq. 4.3} \qquad dF_D = C_D \frac{1}{2}\rho U_{rel}^2 c dr \quad \text{Eq. 4.4}$$

The general form of the thrust (normal force) and torque (tangential force) on an annular rotor section is given by Eq.4.5 and 4.6 respectively. The summation at each annular element can be used to determine the overall thrust and torque for the rotor.

$$dT = \sigma\pi\rho\frac{U_\infty^2(1-a)^2}{\sin^2\varphi}(C_L\sin\varphi - C_D\cos\varphi)r^2 dr \qquad \text{Eq. 4.5}$$

$$dQ = \sigma\pi\rho\frac{U_\infty^2(1-a)^2}{\sin^2\varphi}(C_L\cos\varphi - C_D\sin\varphi)r\,dr \qquad \text{Eq. 4.6}$$

In order to implement this into a CFD solver, a look-up table is used to define the local rotor aerofoil characteristics. Table 2 shows an example of the top level look-up table used to define the NREL 5MW turbine geometry. This includes the chord and twist values for the blades at each radial location as well as defining the specific aerofoils at each of these locations. These aerofoil names then link to secondary tables which define the experimentally obtained lift and drag coefficients for all angles of attack of the relevant aerofoils. These coefficients, along with the chord, twist and local velocity values provide enough information for the solver to calculate the lift and drag forces for each radial rotor section via Eq.4.3 and 4.4. An equal and opposite force is then imparted by the rotor sections on the flow and thus a realistic and geometry dependent force distribution is represented.

### 3.2.5.    **Actuator Line Model**

Thus far the turbine rotor models discussed have represented the turbine rotors as a permeable disk in the flow which assumes an infinite number of infinitely thin blades interacting with the fluid axisymmetrically. Real turbines usually have only two or three rotor blades and as a result the flow is not truly axisymmetric; although at high tip-speed ratios it can be considered a reasonable assumption. [18]Sorensen and Shen's actuator line method attempts to improve on the disk based approximations by representing the body force distributions on each blade along lines through the domain; these lines therefore represent the individual blades in the flow. The three-dimensional Navier-Stokes equations are then solved numerically throughout the flow field. This type of model has also demonstrated the ability to include tip and root vortices in its simulations, which was previously limited in the actuator disk approach.

The geometry of the wind turbine is defined in a Cartesian coordinate system that is based on three key point locations: nacelle, hub and ground. The nacelle point is connected to the ground point by a vertical line, which is then connected to the hub point with a line defined by the turbine's yaw angle and the tilt angle between the horizontal plane and the nacelle axis. This is the line about which the blades rotate. The blades are then defined as a series of points along each blade's axis and each point is the centre of an actuator element. The first blade is defined as a line parallel to the ground (x-y) plane. The other blades are created by using a rotation matrix as follows:

$$\begin{bmatrix} u_x^2 + (1-u_x^2)c & u_xu_y(1-c) - u_zs & u_xu_z(1-c) + u_ys \\ u_xu_y(1-c) + u_zs & u_y^2 + (1-u_y^2)c & u_yu_z(1-c) - u_xs \\ u_xu_z(1-c) - u_ys & u_yu_z(1-c) + u_xs & u_z^2 + (1-u_z^2)c \end{bmatrix}\begin{bmatrix} x_0 \\ x_0 \\ x_0 \end{bmatrix} = [x_1 \quad y_1 \quad z_1]$$

where $c = \cos(\theta)$, $s = \sin(\theta)$, $\vec{u} = u_x\vec{e}_x + u_y\vec{e}_y + u_z\vec{e}_z$ is the unit vector normal to the plane of rotation, $\theta$ is the angle of rotation, and $x_0$, $y_0$ and $z_0$ are the coordinates of the point to be

rotated with $x_1$, $y_1$ and $z_1$ representing the new coordinates of the rotated point. The blades are rotated at each time step by using the angular speed of the rotor. Fig.3 shows a schematic of the discrete ALM actuator elements.



Fig.3 Schematic of blade element points across actuator lines

The approach applies body forces via blade element (BE) methods. The blades are discretized into a number of spanwise elements, each with constant aerofoil, chord, twist etc. As in the BE method, the local velocity of the flow relative to the rotating blade is given by Eq.4.1, at an angle to the rotor plane given by Eq.4.2. Aerofoil look-up tables are again used to calculate the lift and drag forces at each actuator section.

The force on the flow by the turbine must be equal and opposite to these blade forces and so these values are normalised and projected back onto the flow. The total force on a blade element is given by Eq.5.1.

$$F_i^A = \frac{\boldsymbol{dF}}{dA} = \frac{1}{2}\rho U_{rel}^2 c (C_L \boldsymbol{e}_L + C_D \boldsymbol{e}_D) \qquad \text{Eq. 5.1}$$

Gaussian projection of forces was used by [18]Sorensen and Shen (2002) in order to project the calculated aerodynamic forces onto the meshed fluid as a volume force. This is defined by Eq.5.2.

$$f_i^T(r) = \frac{F_i^A}{\varepsilon^3 \pi^{3/2}} \exp\left[-\left(\frac{r}{\varepsilon}\right)^2\right] \qquad \text{Eq. 5.2}$$

where $F_i^A$ is the actuator element force, $f_i^T$ is the force field projected as a volume force, r is the radial distance from the cell centre to the actuator point and $\varepsilon$ controls Gaussian width.

The use of a Gaussian function is required in order to turn the unphysical point forces into a continuous field and thus avoid numerical instabilities from application of forces on discrete blade sections. The ε parameter determines the width of the function and thus plays a vital role in controlling the accuracy of the simulations. The effects of changing this variable have been studied by other parties and it is generally considered acceptable to use a value equal to the characteristic length scale for the blade section under investigation. Also for truly accurate results, the local grid cell width should not exceed half of this value; as suggested by [24]Troldborg (2008). These two conditions will be considered as a guide when choosing values of the ε parameter and also mesh density when setting up actuator line cases.

### 3.3.   *Fundamental CFD Theory*

#### 3.3.1.   **Governing Equations**

[25]The governing equations for fluids consists of a continuity equation (Eq.2.1), a momentum equation (Eq.2.2), an energy balance (Eq.2.3) and a state equation connecting density to pressure. If the fluid is assumed Newtonian as in this case, the equations reduce to

15

$$\frac{\partial \rho}{\partial t} + \frac{\partial \rho u_i}{\partial x_i} = 0 \qquad \text{Eq. 6.1}$$

$$\left(\frac{\partial \rho u_i}{\partial t} + \frac{\partial \rho u_i u_j}{\partial x_j}\right) = -\frac{\partial p}{\partial x_i} + \frac{\partial}{\partial x_j}\left(\mu\left(\frac{\partial u_i}{\partial x_j} + \frac{\partial u_j}{\partial x_i}\right) - \frac{2}{3}\mu\frac{\partial u_k}{\partial x_k}\delta_{ij}\right) + \rho f_i \qquad \text{Eq. 6.2}$$

$$\left(\frac{\partial \rho E}{\partial t} + \frac{\partial \rho u_j E}{\partial x_j}\right) = -\frac{\partial \rho u_j}{\partial x_j} + \frac{\partial u_i \tau_{ji}}{\partial x_j} + \frac{\partial}{\partial x_j}\left(k\frac{\partial T}{\partial x_j}\right) + S_E \qquad \text{Eq. 6.3}$$

In the above equations, $f_i$ is a force applied on the fluid, $S_E$ is an energy source term and the tensor $\tau_{ij} = \mu\left(\partial u_i/\partial x_j + \partial u_j/\partial x_i\right) - \frac{2}{3}\mu\,\partial u_k/\partial x_k$. Equations of state relate pressure $p = p(\rho, T)$ and internal energy $i = i(\rho, T)$ to the variables $\rho$ and $T$, thus allowing the equations to be solved. An example of this relation is the equations of state for an ideal gas, $p = \rho R T$ and $i = C_v T$.

### 3.3.2. **Incompressible Fluids**

At low Mach numbers, compressible effects can be neglected. As such, the continuity equation (2.1) reduces to Eq.7.1

$$\frac{\partial \rho u_j}{\partial x_j} = 0 \qquad \text{Eq. 7.1}$$

[25]There is no need to solve the energy equation as there is no link between the energy equation and momentum and continuity equations. As a result the calculated pressure field is not unique. After simplifying the governing equations using the incompressible condition the system of equations in Eq.7.2 and 7.3 is formed.

$$\frac{\partial \rho u_j}{\partial x_j} = 0 \qquad \text{Eq. 7.2}$$

$$\left(\frac{\partial \rho u_i}{\partial t} + \frac{\partial \rho u_i u_j}{\partial x_j}\right) = -\frac{\partial p}{\partial x_i} + \frac{\partial}{\partial x_j}\left(\mu\frac{\partial u_i}{\partial x_j}\right) + \rho f_i \qquad \text{Eq. 7.3}$$

### 3.3.3. **RANS Turbulence Modelling**

For many cases of turbine modelling, only the time averaged behaviour of the turbine wakes are of interest, which can be approximated as steady state behaviour over time given constant external conditions. It is therefore far less computationally expensive to compute the behaviour using a Reynolds averaged simulation, which produces a time averaged representation of the turbulent behaviour.

To model the Reynolds Averaged Navier Stokes equations, all variables are split into a time-averaged part and a fluctuating part, $\varphi = \bar{\varphi} + \varphi'$. The time-averaged part is calculated as, $\bar{\varphi} = \frac{1}{T}\int_T \varphi(x,t)dt$. For compressible flows often another form of decomposition is done using Favre-averaging. Here variables are decomposed as, $\theta = \tilde{\theta} + \theta''$ where $\tilde{\theta} = \overline{\rho\theta}/\bar{\rho}$. Thus $\theta''$ not only includes the turbulent fluctuations but also the density fluctuations. After Favre averaging the velocity and energy, and performing a standard time-averaging for ρ and p, the following equations are derived.

$$\frac{\partial \bar{\rho}}{\partial t} + \frac{\partial \bar{\rho}\widetilde{u_\iota}}{\partial x_i} = 0 \qquad \text{Eq. 8.1}$$

$$\left(\frac{\partial \bar{\rho}\widetilde{u_\iota}}{\partial t} + \frac{\partial \bar{\rho}\widetilde{u_j}\widetilde{u_\iota}}{\partial x_j}\right) = -\frac{\partial \bar{p}}{\partial x_i} + \frac{\partial}{\partial x_j}\left(\overline{\tau_{\iota J}} - \overline{\rho u_\iota'' u_j''}\right) \qquad \text{Eq. 8.2}$$

Here $\tau_{ij} = \left(\mu\left(\frac{\partial u_i}{\partial x_j} + \frac{\partial u_j}{\partial x_i}\right) - \frac{2}{3}\mu\frac{\partial u_k}{\partial x_k}\delta_{ij}\right)$ and $\overline{\tau_{\iota J}} = \widetilde{\tau_{\iota J}} + \overline{\tau_{\iota J}''}$. For the energy equation a similar transformation is done with the resulting Favre averaged equation

$$\left(\frac{\partial \bar{\rho}\tilde{E}}{\partial t} + \frac{\partial \bar{\rho}\widetilde{u_j}\tilde{E}}{\partial x_j}\right) = -\frac{\partial \bar{p}\widetilde{u_j}}{\partial x_j} + \frac{\partial \overline{u_\iota \tau_{J\iota}}}{\partial x_j} - \frac{\partial}{\partial x_j}\left(\bar{q}_J\right) - \frac{\partial}{\partial x_j}\overline{u_j''p} - \frac{\partial}{\partial x_j}\overline{\rho u_j''E''} \qquad \text{Eq. 8.3}$$

This is the decomposition made in compressible codes. For incompressible codes the Favre decomposition is not used and the RANS equations are derived from the standard time-averaging. For solving the RANS equations, assumptions have to be made regarding the turbulent terms. The exact equations solved are dependent on the models used.

When modelling the governing equations with RANS, the need to model the turbulent scales is apparent. There are several models which deal with turbulence in a variety of manners, making some more applicable in certain cases. Here only the k – ε model was used as the free stream accuracies of this model fit well with turbine dynamics. No boundary layers are included in the simulations and so this model would be expected to provide reliable simulations.

### 3.3.4. **LES Turbulence Modelling**

Large Eddy Simulation is based on the theory of [26]Kolmogorov (1991), that the smallest scales of motion are uniform and the assumption that these small scales serve mainly to drain energy from the larger scales through the cascade process. It was therefore felt that these small scales could be successfully and accurately approximated. The large scales of motion, which contain most of the energy, do most of the transporting and are affected most strongly by the boundary conditions should be calculated directly from the governing equations, while the small scales are represented by a model. This is the basis of LES.

[27]To separate the large scales of motion from the small, some kind of averaging must be done. This is a filter which is a locally derived weighted average of flow properties over a volume of fluid. One of the properties of the filtering process is the filter width, Δ, which is a characteristic length-scale which causes scales larger than Δ (resolved or superGrid Scales (GS)) to be retained in the filtered flow field, while the contribution of scales smaller than Δ (Sub-Grid Scale (SGS)) must be modelled.

Formally, any flow variable, $f$, in LES is composed of a large scale $\bar{f}$, also referred to as grid scales (GS) and a small scale contribution $f'$ related by Eq.10.1.

$$f = \bar{f} + f'. \qquad \text{Eq. 10.1}$$

A filtering operation is then applied to extract the large scale components from all flow variables, which is defined in Eq.10.2.

$$\bar{f}(x) = \oint G(x, x'; \Delta)f(x')dx' \qquad \text{Eq. 10.2}$$

where $\Delta$, in addition to being the filter width, is proportional to the wavelength of the smallest scale retained by the filtering operation. $G$, the filter kernel, is a localised function that satisfies the condition in Eq.10.3.

$$\oint G(x, x'; \Delta)dx' = 1. \qquad \text{Eq. 10.3}$$

These filters vary depending on the LES model implemented but can include Gaussian, top-hat, Fourier cut-off etc. These filtering processes are then applied to the Navier-Stokes equations to obtain the filtered equations of fluid motion, given for incompressible fluids by Eq.10.4 and 10.5.

$$\nabla \cdot \overline{\mathbf{u}} = 0 \qquad \text{Eq. 10.4}$$

$$\frac{\partial \overline{\mathbf{u}}}{\partial t} + \nabla \cdot (\overline{\mathbf{u}\mathbf{u}}) = -\frac{1}{\rho}\nabla \bar{p} + \nabla \cdot \nu\left(\nabla \overline{\mathbf{u}} + \nabla \overline{\mathbf{u}}^{\mathrm{T}}\right) \qquad \text{Eq. 10.5}$$

### 3.3.5. **Subgrid-Scale Modelling**

[26]The subgrid-scale stresses resulting from the filtering operation are unknown and require modelling. Due to small eddies tending to be more isotropic than larger ones it is possible to use simplified methods, like RANS, to simulate them. This method is applied in most Subgrid-Scale (SGS) models. Subgrid-scale turbulent stresses are computed by

$$\bar{\tau}_{ij} - \frac{1}{3}\bar{\tau}_{kk}\delta_{ij} = -2\mu_t\overline{S}_{ij} \qquad \text{Eq. 11.1}$$

where $\mu_t$ is the sub-grid scale turbulent viscosity. The isotropic part of the subgrid-scale stresses $\bar{\tau}_{kk}$ is not modelled, but added to the filtered static pressure term, $\bar{p}$. $\overline{S}_{ij}$ is the rate-of-strain tensor for the resolved scale factor defined by

$$\overline{S}_{ij} \equiv \frac{1}{2}\left(\frac{\partial \overline{u}_i}{\partial x_j} + \frac{\partial \overline{u}_j}{\partial x_i}\right) \qquad \text{Eq. 11.2}$$

Popular SGS models include the Smagorinsky model, the one equation eddy viscosity, and dynamic variants of these, in which the model coefficients can be evaluated mathematically using grid scale information. The Smagorinsky model was used throughout this investigation.

### 3.3.6. **Meshing**

Development of an appropriate mesh for the simulation of rotor flows is crucial to ensure an accurate solution is obtained. Initially, the meshing tool Pointwise was planned to be utilised to generate a high quality mesh with suitable refinement areas around the turbine and wake region. However due to the lack of geometry in actuator model cases this was found to be unnecessary. Instead the standard OpenFOAM tool blockMesh was used to define a rectangular domain surrounding the turbine with cylindrical refinement regions defined using topoSet and

generated using the refineMesh tool. Three levels of refinement were produced, with cylinders of increasing radius having lower cell densities. The result was an efficient mesh for the case with a central high density region containing the turbine and its wake and an increasingly coarse mesh with radial distance from the turbine. Fig.4 shows this typical mesh arrangement.
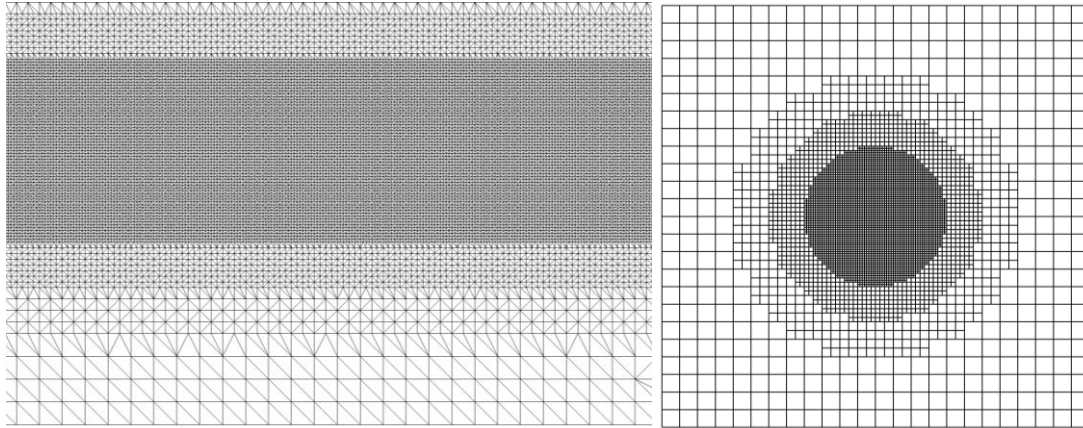


Fig.4 General mesh structure used for all cases, shown as central slices through the XY-plane (left) and the YZ-plane (right)

For the purposes of model comparison, a consistent 3 million cell mesh of this arrangement was used for each of the actuator models. This represented a relatively fine mesh for most cases although the most complex actuator line method is capable of providing more meaningful results given more cells across the rotor diameter. For the validation tests, a global mesh refinement was therefore used to generate an approximate 27 million cell mesh allowing the near wake and blade flows to be resolved with increased fidelity.

### 3.3.7. **Boundary Conditions**

It is important when enclosing a region of interest such as a turbine within a finite domain to consider the effect that the external boundaries may have on the simulation. For this case, it is necessary due to computational cost limitations to keep the domain size tight around the turbine. The effects of the presence of boundaries can therefore be significant if unsuitable conditions are chosen. Slip boundary conditions were used on the sides of the domain to limit the impact of wall presence on the flow dynamics and creating a channelled flow scenario.

## *3.4.* *Data Processing*

### 3.4.1. **Control Volume Power Prediction**

[20]For the kind of complex energy removal associated with turbines, the total thrust force experienced by the turbine can be properly evaluated by calculating the change in flux across the turbine region by applying Conservation of Linear Momentum (COLM) over a control volume. The turbine is enclosed in a rectangular control volume shown in Fig.5 and the momentum flux on each face of the control volume is calculated.
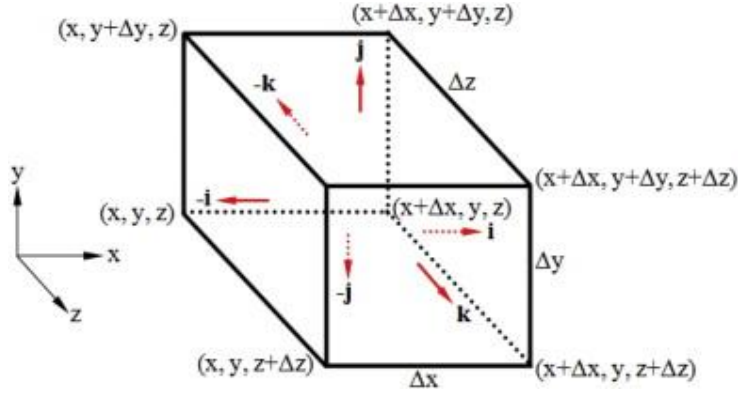
19

Fig.5 Control Volume

Applying COLM over the rectangular control volume, the thrust force acting on the device can be defined by Eq.12.1

$$T = \int_{A_{yz}} [(p)|_x - (p)|_{x+\Delta x}]dA + \int_{A_{yz}} [(pu_x u_x)|_x - (pu_x u_x)|_{x+\Delta x}]dA$$

$$+ \int_{A_{yz}} [(pu_y u_x)|_y - (pu_y u_x)|_{y+\Delta y}]dA$$

$$+ \int_{A_{yz}} [(pu_z u_x)|_z - (pu_z u_x)|_{z+\Delta z}]dA \qquad \text{Eq. 12.1}$$

The power removed by the turbine from the flow is defined using the thrust force as in Eq.12.2.

$$P = T\overline{u_t} \qquad \text{Eq. 12.2}$$

Note that this power removed from the flow is a combination of the useful power that is used to drive the generator and the power loss within the turbine region. In the actuator disk method, the average velocity, $u_t$ , is commonly calculated by averaging the velocity over the area of the disk because of the uniform characteristics of the resistance coefficient.

The axial induction factor, $\propto$ is a measure of the reduction of the velocity at the turbine compared to that of the upstream velocity which is calculated by Eq.12.3.

$$\alpha = \frac{u_\infty - u_t}{u_\infty} \qquad \text{Eq. 12.3}$$

where $u_\infty$ is the far upstream velocity and $u_t$ is the velocity at the turbine.

This is however an imperfect procedure for determining rotor power due to the rectangular nature of the control volume being applied to a system with a cylindrical area of influence. Averaging of the flow velocities over the turbine region is skewed by the corners of the control volume's rectangular faces where the flow is not passing through the rotor swept area and as such becomes marginally larger than the true value. One possible solution to this would be to use a cylindrical control volume which perfectly represents the influence area of the turbine, however this would have to assume the y and z components of velocity are equal in all radial directions, since only a single outer face would be available for evaluation of these radial wake expansion fluxes.; an assumption that would not remain valid if non-axisymmetric features were to be included such as tower or topographical affects.

20

### 3.4.2. **Sampling**

CFD is capable of producing extremely large data sets and extracting the relevant values from these arrays is pivotal to draw supported conclusions about the results. Sampling is a tool that can be used to achieve this. Values can be extracted along lines and across planes through the domain for individual time-steps and given fields obtained during the solution. This method will be used to obtain graphical representations of the actuator force distributions and velocity traverses including wake and upstream radial velocity profiles at various locations and axial traverses for both inter-model comparisons and experimental validations.

### 3.4.3. **Visualising Turbulence**

The highest fidelity transient solvers for wind turbine dynamics would be expected to include accurate approximations of the turbulent flow behaviour surrounding the turbine, both in the near and far wake regions. Real turbine wakes experience a variety of interesting turbulent behaviour. In the far wake, the faster flowing free stream fluid outside of the wake region interacts with the slower wake flow creating shear strains between the layers of fluid. As a result, turbulent eddies form and the far wake flow becomes unstable with large perturbations. It is therefore imperative that the LES and transient modelling is set up correctly as to properly resolve this behaviour.

In the near wake region of real turbines, the interaction of the rotating blades with the oncoming fluid creates vortex structures within the wake and vortex shedding at both the root and tip of the rotor blades. Due to the requirement of separate blade representations, only the more complex actuator line models are capable of simulating this behaviour, but in these the turbulent modelling techniques applied are responsible for assuring accurate simulations of the vortex structures.

There are a few different ways of observing the predicted turbulent behaviour from the turbine models and assuring that they have been properly resolved. The second invariant of the velocity gradient tensor can be used as a visualisation tool for turbulence or to identify vortex flow structures and is calculated throughout the computational domain to be represented using an isosurface contour. The second order velocity gradient tensor $D_{ij}$ can be shown to comprise of a symmetric $S_{ij}$ and a skew-symmetric $\Omega_{ij}$ part, where the rate-of-strain tensor $S_{ij}$ is defined in Eq.9.2 and the vorticity tensor $\Omega_{ij} = \frac{1}{2}(\frac{\partial u_i}{\partial x_j} - \frac{\partial u_j}{\partial x_i})$. The characteristic equation for $\nabla u$ is then given by Eq.13.1

$$\lambda^3 + P\lambda^2 + Q\lambda + R = 0 \qquad \text{Eq. 13.1}$$

P, Q and R represent the three invariants of the velocity gradient tensor. Using the symmetric and anti-symmetric decomposition, the second invariant Q, can be expressed by Eq.13.2.

$$Q = \frac{1}{2}\big(tr(\bar{D})^2 - tr(\bar{D}^2)\big) = \frac{1}{2}\|\bar{\Omega}\|^2 - \|\bar{S}\|^2 \qquad \text{Eq. 13.2}$$

The second invariant of the velocity gradient tensor Q can therefore be numerically obtained directly from the velocity field and as such is included as a computed field within the model using the C++ formula:

$$Q = 0.5*(sqr(tr(fvc::grad(U))) – tr(((fvc::grad(U))\&fvc::grad(U)))))$$

As described by [28]V'aclay (2007), the Q-criterion defines a vortex as a "connected fluid region with a positive second invariant of $\nabla u$, i.e. Q > 0. Since Q represents the local balance between shear strain rate and vorticity magnitude, the Q-criterion defines vortices as areas where the vorticity magnitude is greater than the magnitude of rate-of-strain. A second condition is included in the Q-criterion relating to the local pressure, requiring it to be lower than the ambient pressure within the proposed vortex region. This Q-criterion can be utilised in analysing the predictive accuracy of the implemented actuator line model for vortex simulation.

### 3.4.4.    **Quantifying Computational Expense**

There is no standard index in the literature that is used to quantify computational expense. Often if the hardware setup on which the models are used is kept consistent, the time taken to solve a particular case can be used to benchmark the performance of a model. This method was utilised within this investigation in order to quantitatively compare the speed of each model for the given case defined in section 2.4.1.

All cases were run on a computer with server architecture using four Intel(R) Xeon(R) X5690 processors, each running at a clock speed of 3.47 GHz. A substantial amount of RAM (50 GB) was available for it to not be a limiting factor on the speed of these CPU intensive calculations. Only four of the twelve available processors were used to run each case, allowing them to utilise 100% of these processors while other applications were run on the remaining processors.

# 4. Model Results, Comparisons and Validation

## *4.1.    Comparison Case Study: NREL 5MW Reference Turbine*

The NREL defined 5MW offshore wind turbine was used to carry out direct comparisons between each of the models. This hoped to identify the shortcomings of the more commonly used simpler forms of actuator models against the more recently developed and more complex forms. Also conversely, this comparison allows the improvements that these more complex forms of actuator models can provide to be established.

### 4.1.1.    **Radial Force Distributions**

The method used to distribute the rotor equivalent volume forces across the actuator region presents the largest contributor to their complexity. The theory behind the distribution techniques used by each model has been discussed in section 3.2. The resulting model simulations allow the volume forces across the actuator region to be visualised and the increase in complexity from one model to the next to be recognised; as summarised in Fig.6.

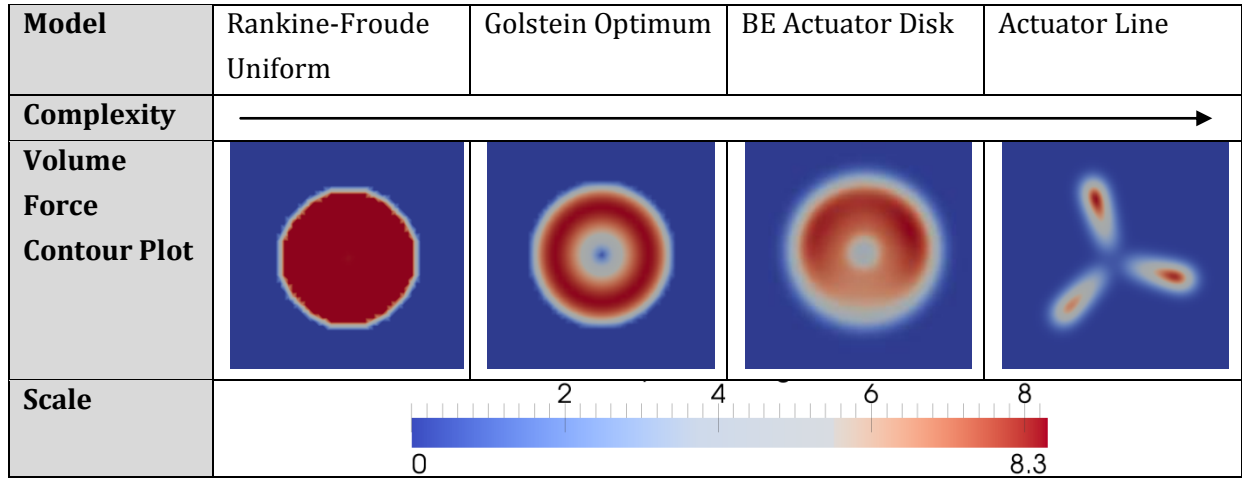| Model | Rankine-Froude Uniform | Golstein Optimum | BE Actuator Disk | Actuator Line |
|---|---|---|---|---|
| **Complexity** | ⟶ | | | |
| **Volume Force Contour Plot** | | | | |
| **Scale** | | | | |

Fig.6 Model axial force distributions

The radial distribution of volume forces in both the axial and tangential directions can be plotted for each of the distribution models; as represented in Fig.7. This allows the distributions to be compared and the complexities to be observed. The BEM covers both BE Disk and ALM since both models use the same distribution method.
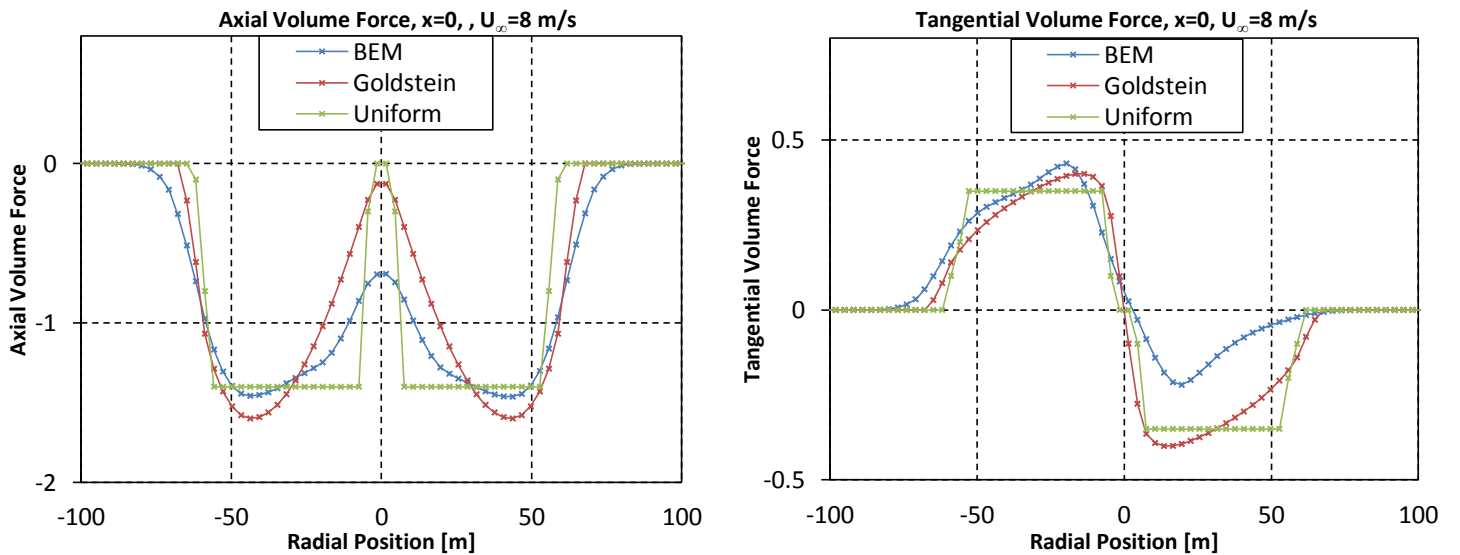


Fig.7 Radial distributions of axial and tangential rotor forces

### 4.1.2. **Far Wake Profile Prediction**

Accurate prediction of the far wake profile behind a turbine is necessary for modelling of turbine arrays. The influence of wake interactions must be correctly represented to understand how energy shadowing of an array of turbines influences energy extraction by the individual turbines. In order for this to be achievable the individual turbine representative models must be capable of accurately predicting the downstream wakes.

The transient wake behaviour was simulated using each of the models in LES, which resulted in snapshots of the unsteady wake development to be obtained. Fig.8 shows snapshots of the wake development profile behind the NREL 5 MW turbine at 5 minute intervals after turbine activation, with the final image showing the fully developed wake. These simulations were produced using the Blade Element Disk and Actuator Line models.
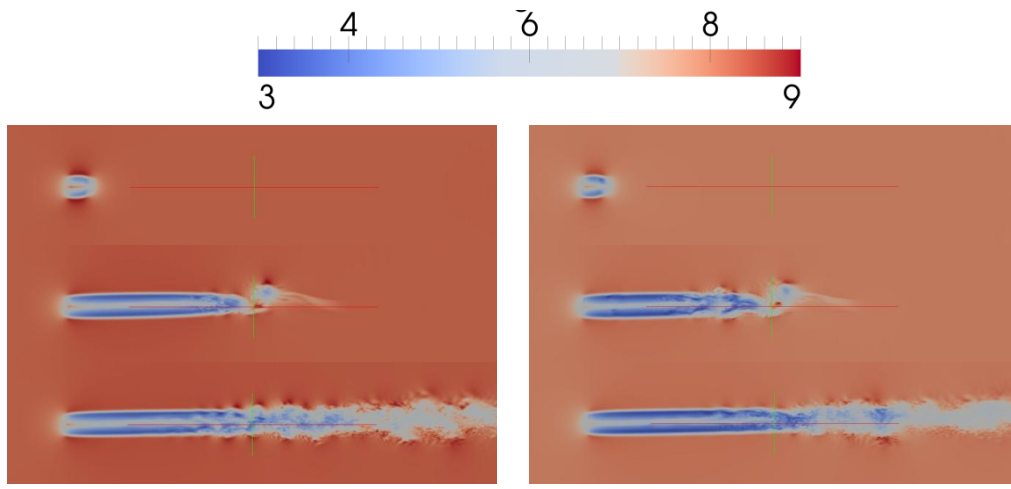
Fig.8 – Transient LES wake development at 5 minute intervals from turbine activation as simulated by BE Disk model (left) and ALM (right).

In order to compare the predicted far wake profiles, the mean velocities were also calculated. Fig.9 shows a time-averaged wake obtained using the ALM.
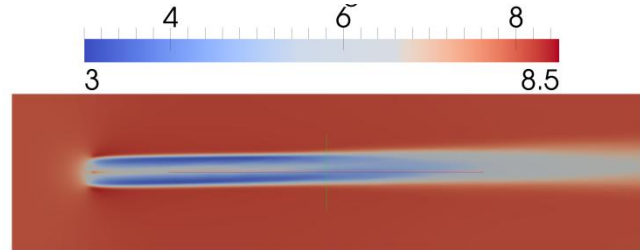


Fig.9 Time-averaged wake predicted by the LES actuator line model

The far wake region is defined as beyond one turbine diameter downstream of the turbine. This region is considered far enough downstream to be independent of the specific rotor geometry and not be influenced by rotor angular velocity. The span-wise mean velocity profiles were sampled for each model at distances of 2D, 8D and 16D, where D is the diameter of the turbine; this is presented in Fig.10. The BE Disk model produced identical far wake results as the ALM and so was omitted from the graph.
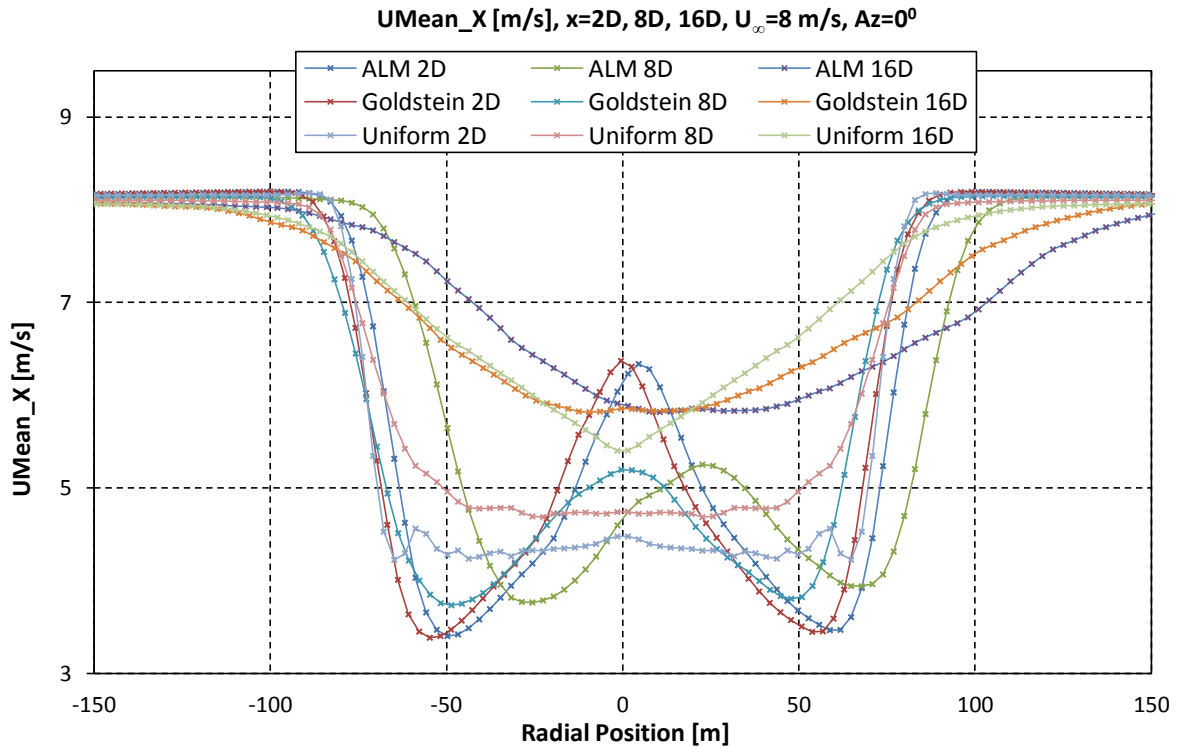
**UMean_X [m/s], x=2D, 8D, 16D, $U_\infty$=8 m/s, Az=$0^0$**



Fig.10 Far wake mean velocity profiles at downstream distances of 2D, 4D and 6D

### 4.1.3. **Near Wake Profile Prediction**

The ability of the various models to simulate the behaviour of the near wake region was assessed. This region is defined as within one rotor diameter downstream of the turbine and is said to be influenced significantly by the rotor angular velocity and the geometry of the blade. Fig.11 shows the wake profile data obtained from each of the models at 0.25D downstream of the turbine.
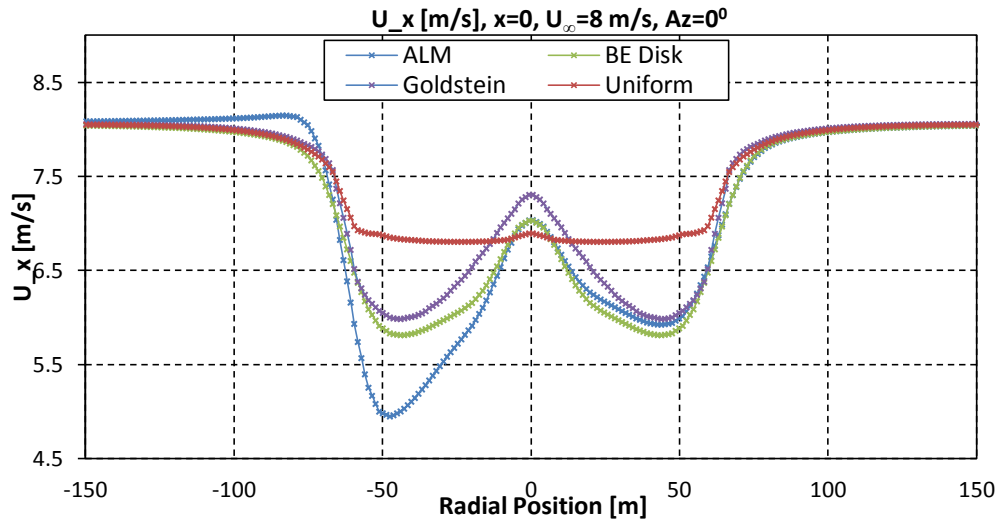


Fig.11 Velocity profiles along the centrelines of the actuator model rotors

Contour plots of the velocity on the rotor plane were obtained for each model to provide an image representation of the near wake flow predictions. These are presented in Fig.12.

| Model | Rankine-Froude Uniform | Goldstein Optimum | BE Actuator Disk | Actuator Line |
|---|---|---|---|---|
| Complexity | | | | |
| Rotor Plane Velocity Contour Plot | | | | |
| Scale | | | | |
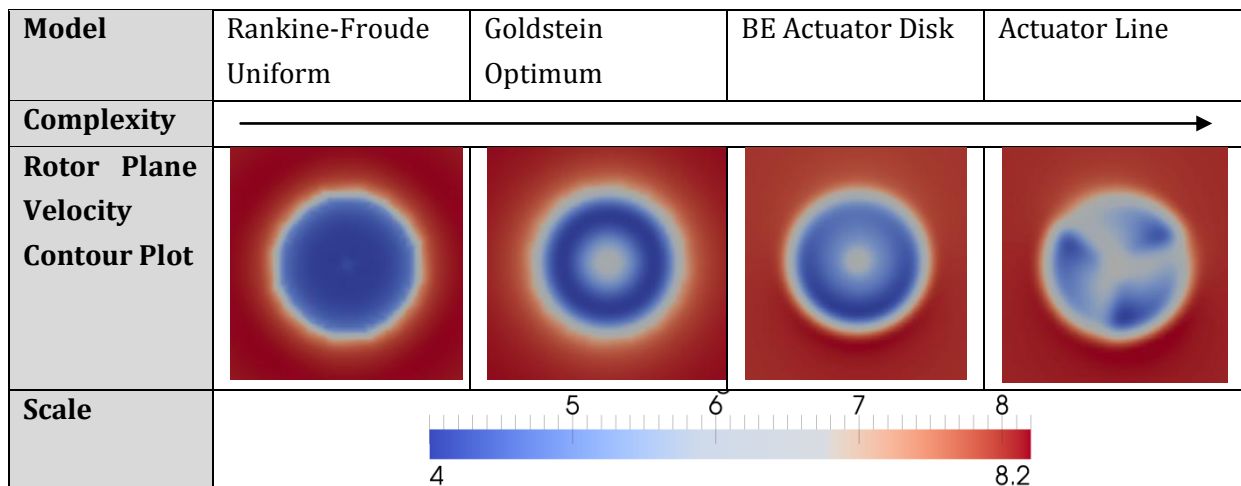
Fig.12 Velocity contours on the rotor plane for each model

### 4.1.4. **Rotor Power Prediction**

The Rotor power predicted by each of the actuator models was obtained using a consistent setup of the control volume method described in section 3.4.1. The turbine was assumed to operate at its rated value of 12.1 rpm at 8 m/s. For the simpler models where a total thrust and torque is prescribed instead, the values were obtained from the computed total thrust and torque calculated by the actuator line model. This model uses a discrete blade

element approach to obtain local force values and then sums these to obtain total forces over the entire blade; thus approximating an integral of the true radial distribution of local forces. This can therefore be considered an analytical BEM approach that could be obtained manually without the use of the actuator line model, and thus represents a reasonable method of quantifying the total force values, even if only the simple disk models were available. This allows all the models to be provided with equivalent input data. The rotor power over time was then quantified for each model and is presented in Fig.13.
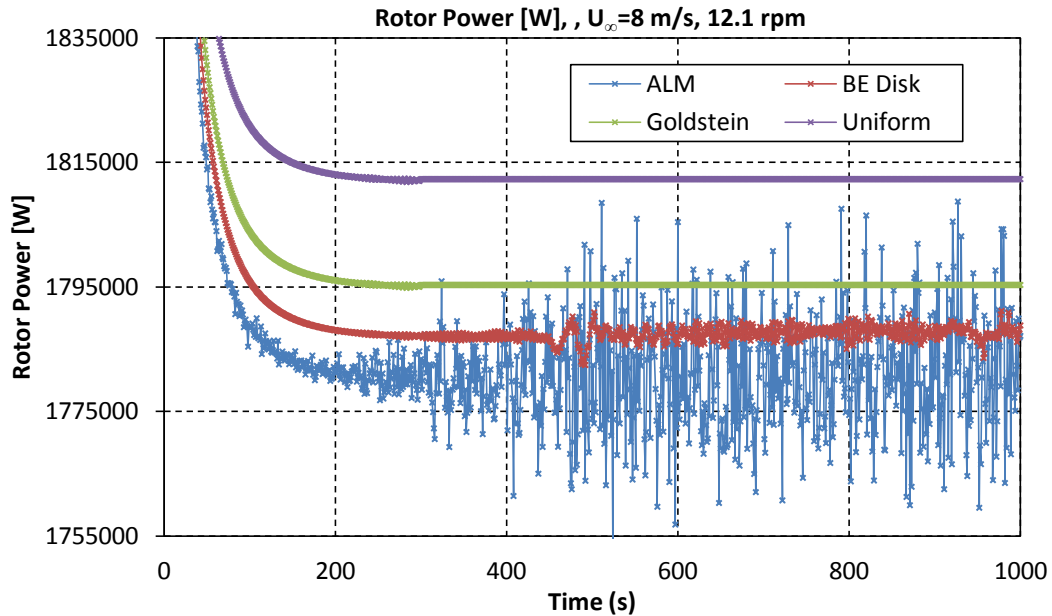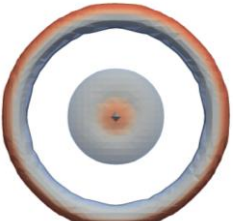


Fig.13 Rotor Power over time predicted by each model.

### 4.1.5.   **Simulation of Turbulent Structures**

The second invariant of the velocity gradient tensor Q was used to analyse the ability of the models to simulate turbulent structures. As described in section 3.4.4, a positive value of Q suggests the presence of vortex flow. A Q isosurface was produced for each model to aid in visualisation of the predicted turbulent structures. The peak Q values predicted by each model and the Q=0.0025 isosurfaces are presented in Fig.14 and coloured by velocity magnitude.

| | | |
|---|---|---|
| Fig.14.1 Uniform Disk Turbulent Structures, Q max =0.0554 |  |  |
| Fig.14.2 Goldstein Disk Turbulent Structures, Q max =0.0554 |  |  |

26

| | | |
|---|---|---|
| Fig.14.3 BE Disk Turbulent Structures, Q max =0.164, |  |  |
| Fig.14.4 ALM Turbulent Structures, Q max = 0.133, |  |  |
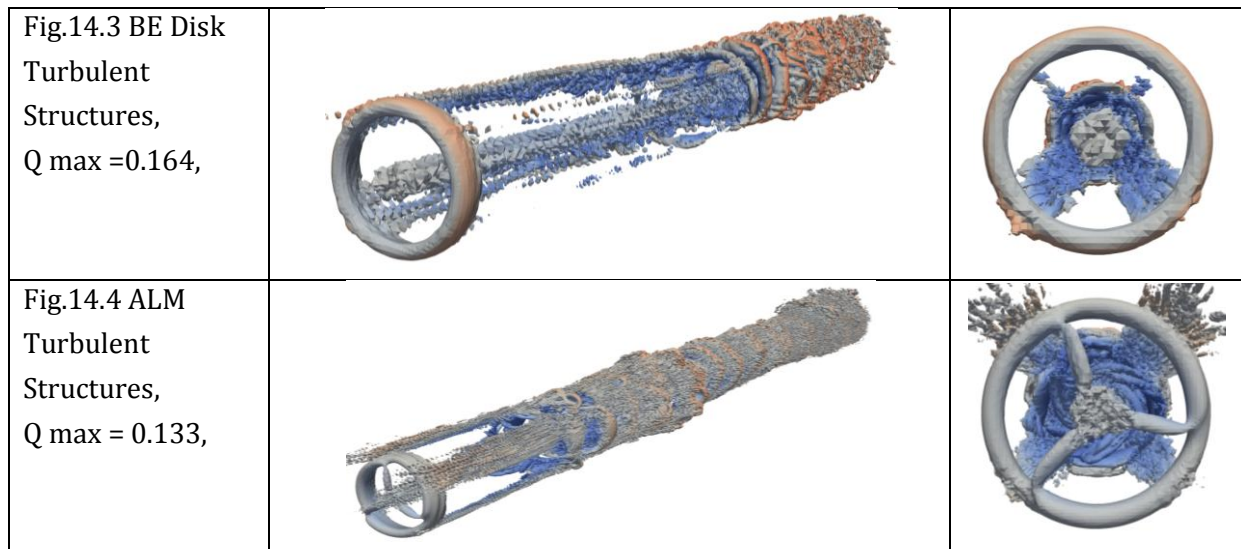
The actuator line model is capable of simulating root and tip vortex shedding. This is particularly observable in the early stages of turbine operation, as shown in Fig.15.
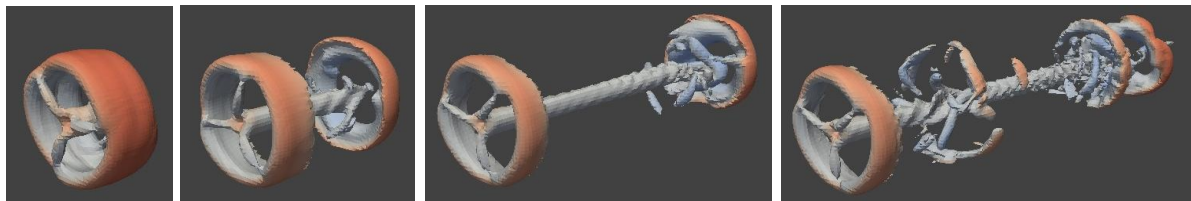


Fig.15 Root and tip vortex shedding simulated by the ALM.

### 4.1.6. Computational Expense

The efficiency with which each model can obtain a solution is important in analysing the suitability of the models for particular applications. For example, a solver with an extremely high computational expense will not be applicable to cases involving large arrays of wind turbines as the cost of the hardware required to obtain a solution within an acceptable time scale would be too great. There is always a trade-off within CFD between accuracy, speed and stability therefore the models that produce the best solutions are expected to take longer to obtain that solution and also operate well for fewer cases. The run time for each solver on a consistent case and on consistent hardware was used as a measure of computational expense and this is quantified in Fig.16. The cases were run using LES for 1000s and with a time-step of 0.0333s and the solvers were set up to compute all the same fields for the entire domain.

| Model | Run Time (s) | Run Time (hours) |
|---|---|---|
| Uniform | 331442 | 92 |
| Goldstein | 349234 | 97 |
| BE Disk | 448122 | 125 |
| Actuator Line | 485943 | 135 |
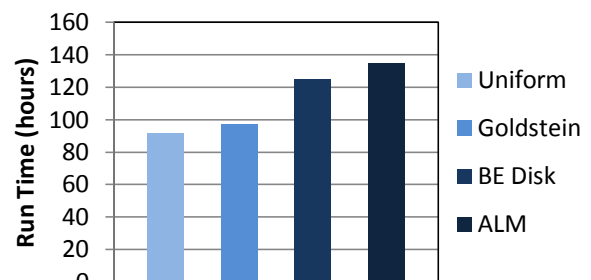


Fig.16 Equivalent run times for all models.

### 4.1.7. **Modelling of Multi-turbine Interactions**

Due to the limitations on time, this project mainly analysed the model performance when simulating single turbine behaviour. However, since most industrial modelling applications are concerned with the behaviour of large arrays with turbines that interact with the wakes of other upstream turbines, the suitability of the more complex actuator modelling techniques should be assessed for this kind of application. Other individuals operating within the group project have made use of the Goldstein optimum distribution actuator disk for modelling of turbine arrays as its low computational cost allows for a large domain containing many turbines to be simulated.

The ALM was used to simulate the interacting behaviour of two of the NREL defined turbines, with the second operating 1.8km downstream of the first and the rotor swept areas overlapping by 0.5D. A plot of the flow interactions predicted by the model is presented in Fig.17 with boxes identifying the two turbine locations.
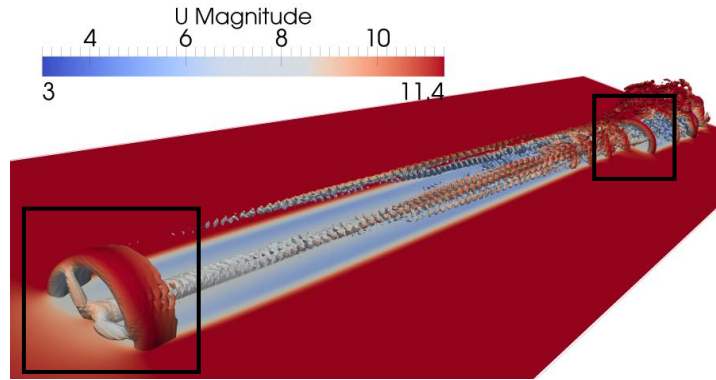


Fig.17 Multi-turbine interactions simulated with the ALM

Fig.18 shows the span-wise mean flow profiles through the centreline of the upstream and downstream turbine predicted by the ALM model.
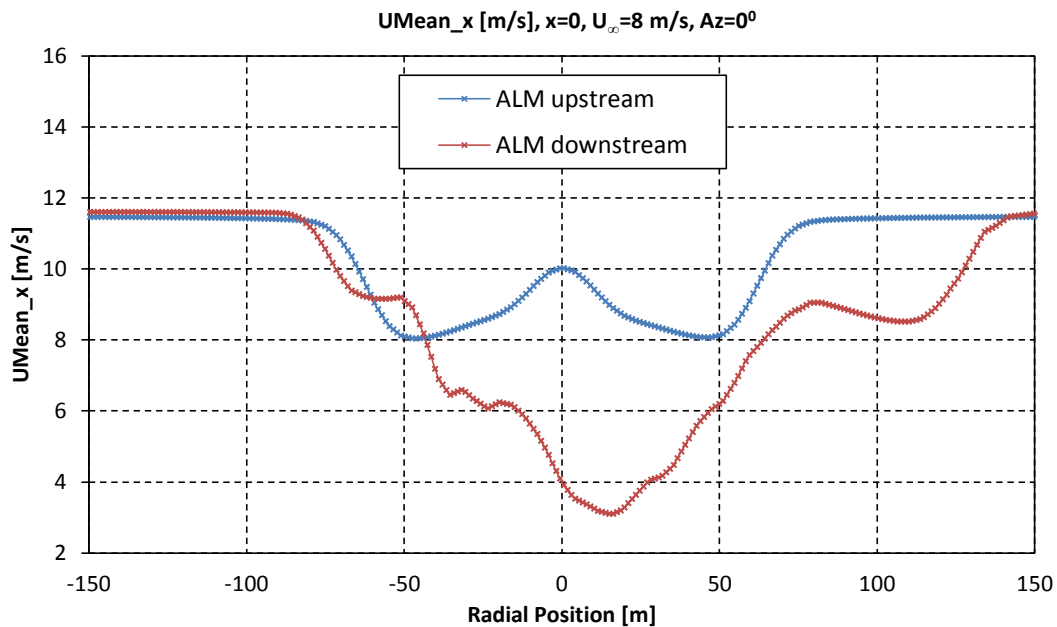


Fig.18 Span-wise mean velocity profiles for upstream and downstream turbines.

28

## 4.2. Validation Case Study: MEXICO Experiments

By using the implemented actuator line model set up to match the case for the MEXICO wind tunnel experiments, the induced velocity can be calculated in points of the external domain. Comparisons with experimental data coming from PIV measurements have been performed. For these tests, three values of wind speed have been used and all three components of velocity computed for axial traverse and radial traverse measurements.

### 4.2.1. Upstream Velocity Traverse Comparisons
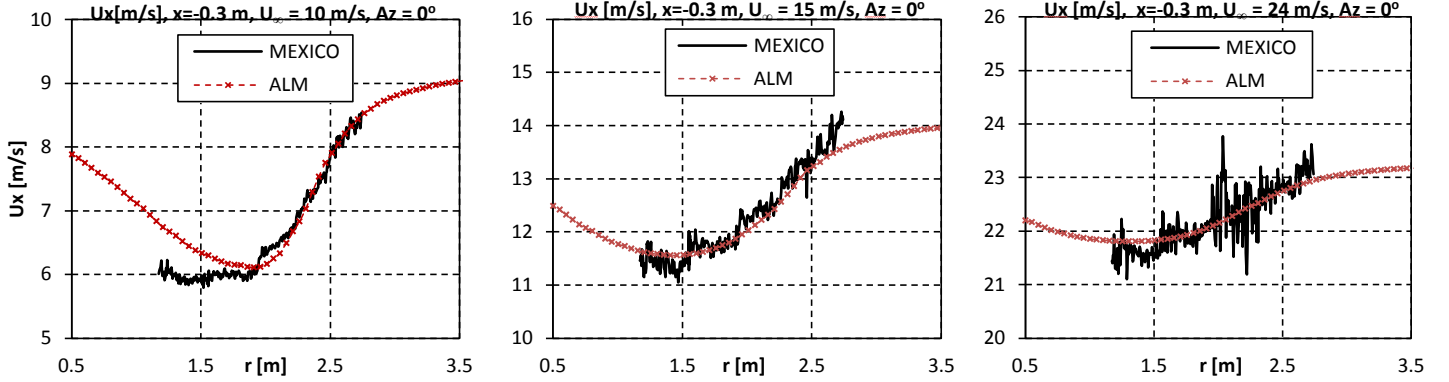


Fig.19 Upstream radial velocity traverse, axial component at 10, 15 and 25 m/s
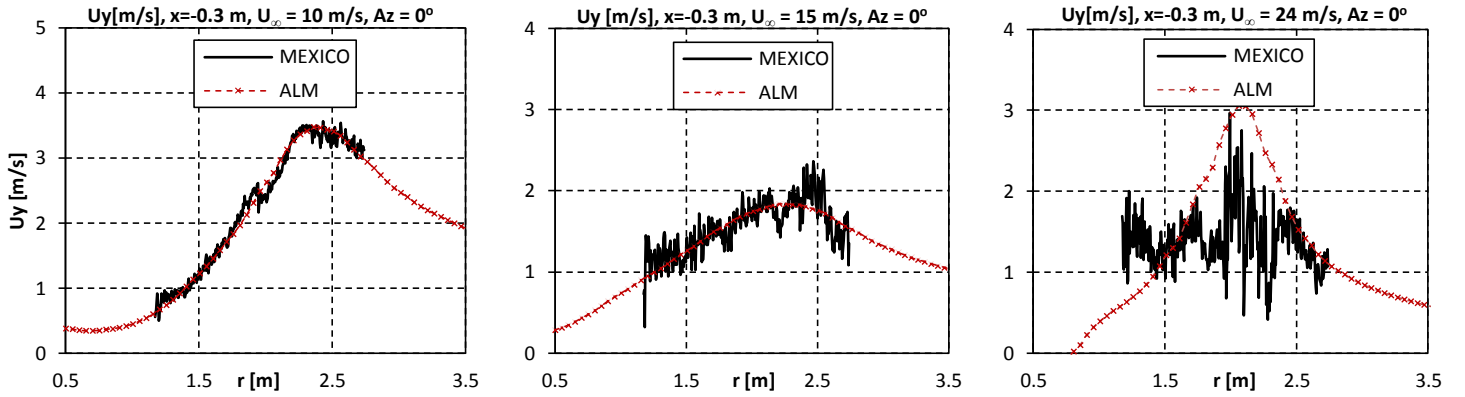


Fig.20 Upstream radial velocity traverse, in-plan horizontal component at 10, 15 and 25 m/s
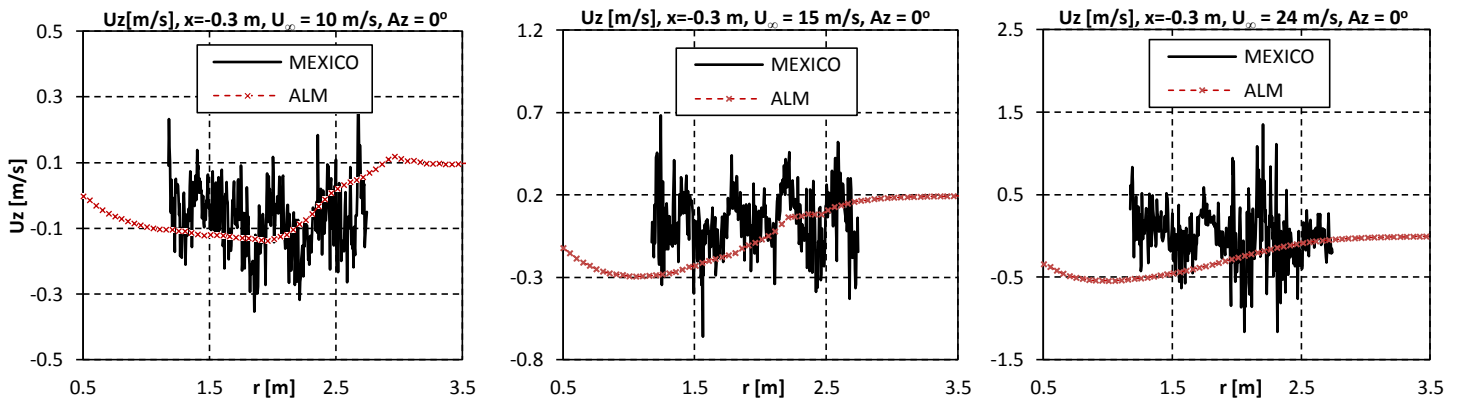


Fig.21 Upstream radial velocity traverse, in-plan vertical component at 10, 15 and 25 m/s

### 4.2.2. **Downstream Velocity Traverse Comparisons**
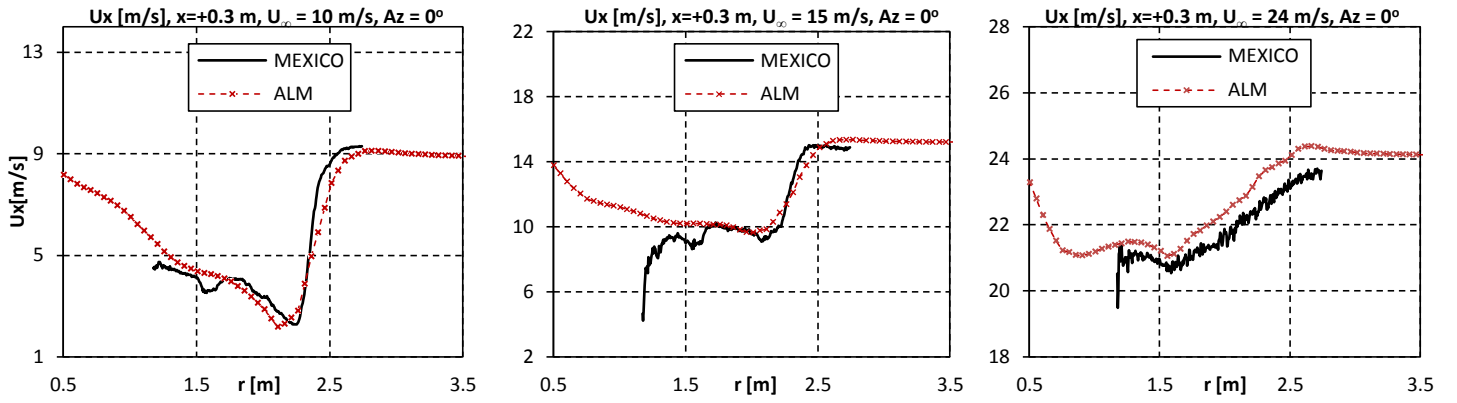


Fig.22 Downstream radial velocity traverse, axial component at 10, 15 and 25 m/s
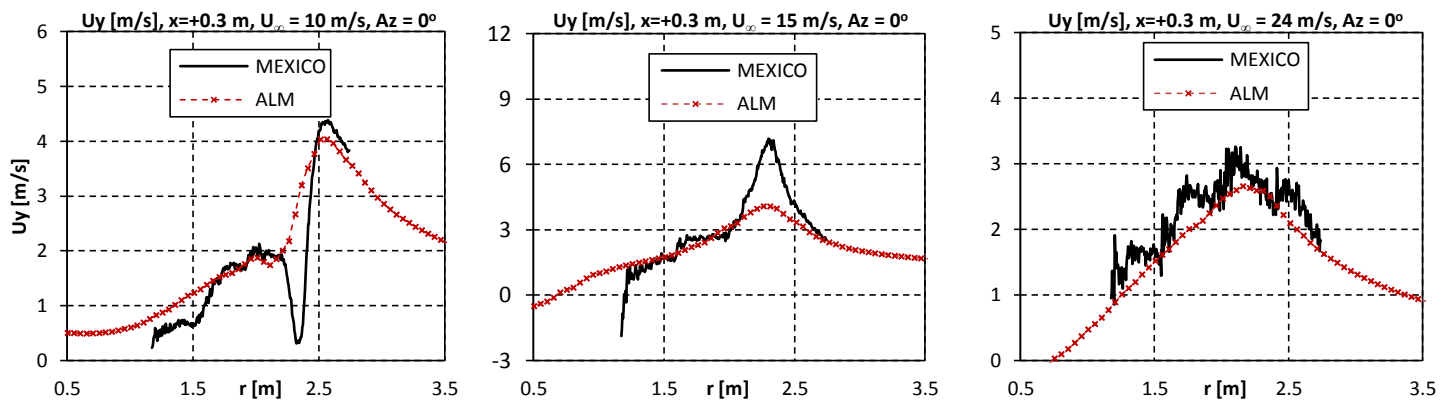


Fig.23 Downstream radial velocity traverse, in-plan horizontal component at 10, 15 and 25 m/s
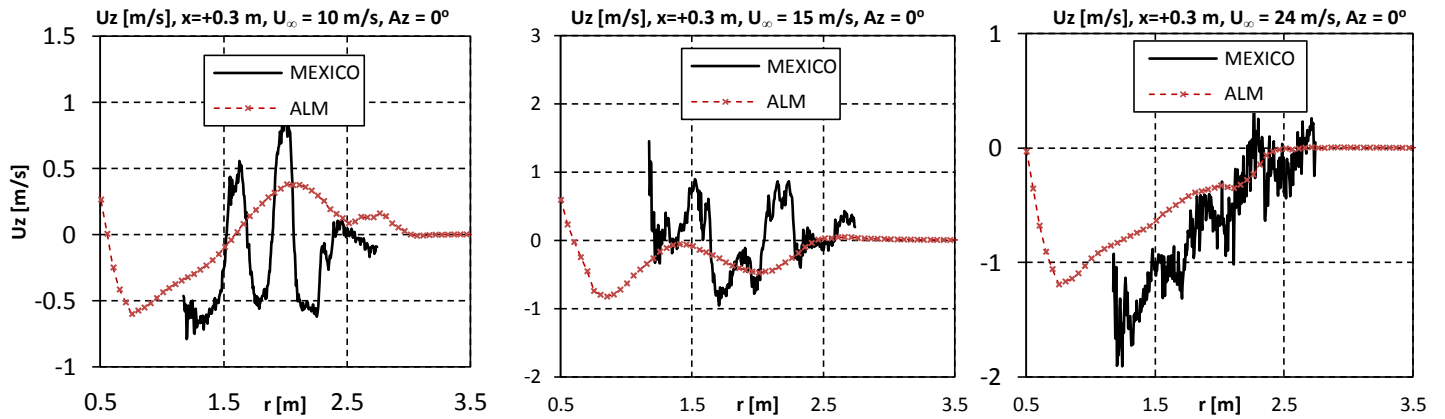


Fig.24 Downstream radial velocity traverse, in-plan vertical component at 10, 15 and 25 m/s

### 4.2.3. **Axial Velocity Traverse Comparisons**
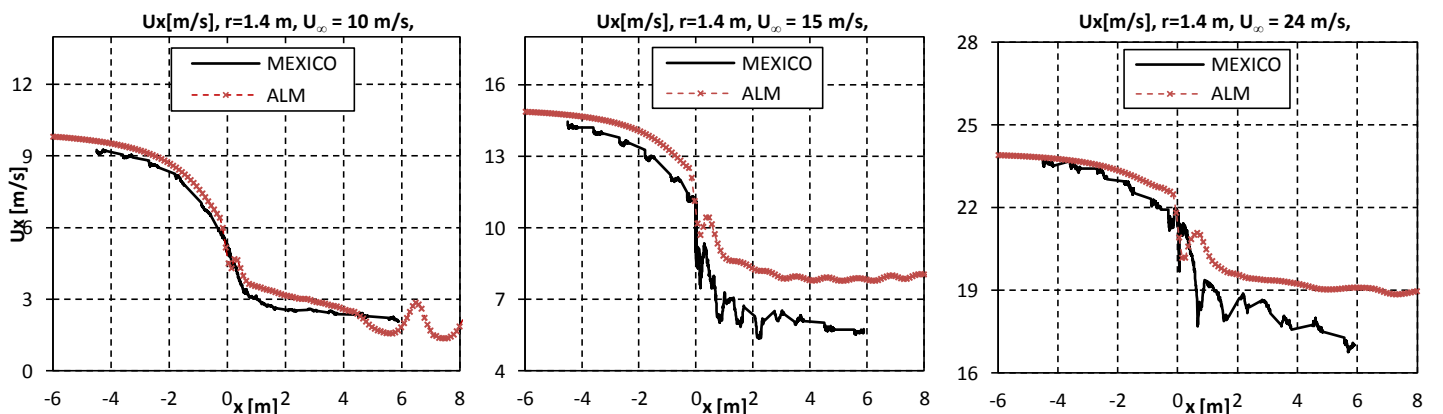


Fig.25 Axial velocity traverse at 1.4m radial position, axial component at 10, 15 and 25 m/s
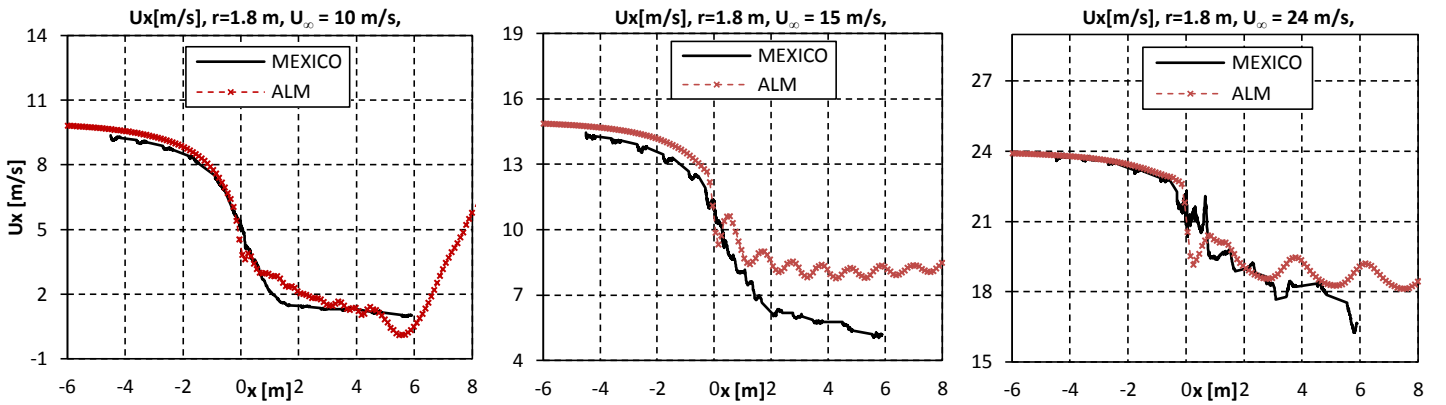
Fig.26 Axial velocity traverse at 1.8m radial position, axial component at 10, 15 and 25 m/s

# 5. Discussion and Conclusions

## 5.1.    *Discussion of Model Comparison*

### 5.1.1.    **Radial Force distribution**

The uniform model, analogous to the Rankine-Froude analytical theory was found to only be useful for approximating global momentum loss across the turbine. The model represented the entire length of the blades as providing an equal force on the flow and did not represent the turbine hub. This provided a total retarding force on the flow that is equivalent to that of a real turbine but the local magnitudes were not resolved.

The Goldstein model distribution was based on the theory of Betz and represents an ideal turbine distribution. Real turbines are not ideal, although the comparisons with blade element distributions show that the NREL rotor has similar distribution to that predicted by Goldstein's optimum. This distribution allowed the cylindrical blade region close to the hub to be represented as providing a lower force, unlike in the uniform model, and also represented the hub as providing no force.

The Blade Element disk was able to represent the expected blade forces for the specific rotor geometry. Validation showed this model to be an accurate approximation of the experimentally observed rotor forces for the MEXICO rotor and thus for other rotor geometries such as the NREL 5 MW comparison case. This stands for both axial and tangential force components. The ALM used the same method as the BE Disk but allowed the forces to be distributed on lines allowing simulation of discrete blades. The tangential forces were not equal and opposite on advancing and receding sides as in the simpler models but instead different magnitudes were observed between the two sides of the turbine as a result of the individual blade locations at the time of sampling. This suggests a more accurate turbine representation.

### 5.1.2.    **Far wake**

In the far wake region, the flow behaviour is generally considered to have developed for long enough away from the turbines influence to become independent of the rotor geometry and angular velocity. Thus it was hypothesised that the models would predict relatively similar results with regards to the far wake velocity profiles given identical turbulence modelling setups. This was found to be a fairly accurate hypothesis with the BE Disk and ALM model

31

producing identical wake profiles in the far wake region, the Goldstein Optimum model produced an almost identical wake profile however the assumption of axisymmetry prevented the wake from deviating from the axis of rotation, as was observed in the ALM simulation. Even the heavily simplified uniform model produced a close approximation of the far wake flows as shown in Fig.10.

### 5.1.3. **Near wake**

The near wake region is considered close enough to the turbine to be dependent on the specific turbine geometry and to be heavily influenced by the angular velocity of the turbine. This was particularly noticeable from the uniform model as its excessive simplification of the turbine forces prevented it from being able to accurately predict the velocity profile in this area. The Goldstein optimum model, having a better approximation of turbine force distributions was more capable however it still did not match that of the Blade Element. The BE disk predicted the profile well due to its geometry specific force distributions but due to its axisymmetry, it, along with the other axisymmetric models, predicted all the near wake flows as if a blade was in the same relative position. The ALM did not have this problem due to its simulation of the individual rotating blades and thus the gaps between blades were also represented. Therefore it represents an improved near wake prediction model. This is clear from the axial asymmetry of the velocity contour of the ALM in Fig.11.

### 5.1.4. **Rotor Power**

Using the control volume technique, the rotor power predicted by each of the models for a range of free stream velocities was obtained. The results showed that with increase in model complexity, the predicted rotor power decreased. Also with complexity increase, the fluctuations in instantaneous rotor power increased. The variation in the near wake flows created by modelling of the individual blades in the ALM is responsible for this level of fluctuation. The uniform model predicted a considerably higher rotor power with its averaged settled value being 1.628% larger than the ALM, whilst the Goldstein and BE Disk were relatively close to the ALM with average settled rotor power 0.675% and 0.377% larger respectively. Although these values seem fairly small, this can account for a large difference in total energy generation over the active life of the turbines.

### 5.1.5. **Turbulent Structures**

The Q-criterion was used to analyse the turbulent structures formed by the activity of the actuator models. All models were capable of inducing vorticity in the wake through application of torque forces and thus positive values of the second invariant of the velocity gradient tensor were present in all cases. The maximum values varied between models by around 33.8% and the BE Disk model predicted the largest values. The isosurface plots at Q=0.0025 were useful for visual comparisons of the turbulent structures present in the simulations. As previously stated, the assumption of axisymmetry made by all but the ALM model restricted their ability to simulate root and tip vortex separations although the disk

models were still able to create turbulent bands due to the shear between the actuator region and free stream flow. The Q contour for the ALM in Fig.14.4 shows the individual blade shear.

### 5.1.6. **Computational Expense**

The observed difference in run times between models was not as great as previously predicted for a consistent case. Since the mesh used was particularly fine and solving the same fields over the whole domain in LES contributes to the majority of the run time, the differences in efficiency of the different models was somewhat disguised. This does not however mean that the complex ALMs are not significantly more computationally expensive. The simpler disk models which resolve less of the complex flow physics are more forgiving of a coarser mesh and an extremely fine mesh does not improve the model behaviour. This is where the increased efficiency comes from in real applications, as a coarser mesh can be used when solving with simple disk models. This makes them more suitable for simulation of large turbine arrays. The ALM was shown however to be more capable at simulating multi-turbine interactions due to its ability to simulate the near rotor flow physics more completely. Its requirement for a fine mesh to properly resolve this behaviour however limits the ability to model large arrays.

## *5.2. Discussion of Model Validation*

### 5.2.1. **Relevance of the case**

Due to the projects focus on offshore wind turbines, as these represent the primary industrial application, the models are expected to predict the behaviour of the largest turbine rotors, which operate at low RPMs. The MEXICO rotor case used as validation is an example of a fairly large scale experimental case, however the rotor is still only approximately 1/25th the size of an offshore turbine such as in the NREL comparison case. This also means that the rotational speed of this validation case is over 35 times that of the rated operating RPM for the offshore scale turbine. This difference is likely to have a large effect on the turbine behaviour and thus the models ability to accurately represent it. Although the ALM showed good agreement with the MEXICO PIV data, the model was developed with full scale offshore turbines in mind and thus would be expected to perform better for the slower blade speeds that are involved in full scale offshore cases. This would greatly accentuate the need for modelling of individual blades since high RPMs make an assumption of axial symmetry more valid.

### 5.2.2. **Radial Traverses**

The ALM consistently predicted the radial variations in the axial and in-plan horizontal components of flow in the external field of the MEXICO rotor. As expected the ALM did not predict the fluctuations present in experimental observations. This may be because of the lack of a random turbulent inlet condition which would be present within the wind tunnel but also may be the result of inconsistency in the wind tunnel flow conditions. Also, in the ALM, the velocity profiles were all sampled at one instant in the simulation, where the PIV data may have been collected over a period of time, thus being affected by the transient unsteady flow. The

average predicted values were however a good match. For the in-plan vertical components of flow, the ALM performed less well. A better understanding of the experimental data may be required to identify the reasons for this, although the performance of the ALM would be expected to be better for lower blade speeds.

### 5.2.3. **Axial Traverses**

The ALM showed a good ability to predict the velocity deficit across the rotor plane. Due to the amount of time taken to solve this case with a fine enough mesh (27 million cells) to properly resolve the rotor region and fulfil the epsilon parameter requirements stated in section 3.2.5, these axial traverses were sampled after only 1.5 seconds of turbine operation. This resulted in the wake not being fully developed within the sampled region and thus the velocity deficit is not fully formed and large eddy fluctuations are still present within the sampled wake region. These would be expected to settle over time as the wake develops further downstream and thus the model approximation would be expected to improve.

## *5.3.    Project Conclusions*

The uniformly distributed actuator disk was a poor representation of true wind turbine behaviour. Although it remains valid for approximation of the mass momentum transfer process, its extreme oversimplified representation of the rotor means that an engineering wake model or analytical approach would provide just as much insight into turbine flow dynamics. As a result this model is not appropriate for industrial wind farm modelling applications.

The Goldstein Optimum model was proved to represent real turbines well, since most modern day turbines are designed based on achieving as close to this theoretical distribution as possible. This model commonly used in industry was able to approximate the near rotor flow profiles almost equally to the BE approach and as a result its rotor power prediction was quite close to that of the highest fidelity ALM. The main issue with prescribed radial distribution models of this type is there assumption of axisymmetry, which excludes the blade dependent near wake effects and presence of complex turbulent structures such as vortex shedding, all of which contribute to accurately predicting the rotor power. It can therefore be concluded that the use of simple actuator disk models does substantially contribute to inaccuracies in wind farm power prediction as an overestimation of 0.675% was observed in this investigation.

Actuator line models were shown to provide substantially more complete representations of true turbine dynamics due to the removed assumption of axisymmetry. This allowed the more complex near wake flow characteristics of real turbines to be simulated. This high fidelity actuator model predicted the lowest rotor power of all the models and high confidence can be put in this approximation as a result of the model validation. The main issue with the potential for use of this model in industry is its requirement for a very fine mesh, resulting in a large computational expense. Although it proves very useful for simulation of single turbines or two interacting turbines, its application to modelling of large arrays is not viable given today's restrictions on computing power. It may therefore be good practise to model a single geometry specific turbine with an ALM and model large arrays with Goldstein or

some other prescribed radially distributed disk. An adjustment coefficient can then be applied to power outputs, obtained from comparisons to the ALM.

In summary, the use of simple actuator disk models can result in inadequate estimates of the rotor power. More complex actuator models have the potential to reduce these inaccuracies but their applicability to industrial cases is limited by their large computational expense. Actuator models in general have great potential for providing an improved solution over current wind farm predictive techniques.

## *5.4.*     *Further Work*

### 5.4.1.   **Further Analysis Work**

Another model that has been explored recently is the Actuator Surface Model (ASM). This calculates the forces on a 2-D airfoil as a function of the chord, avoiding one of the major simplifications of the ALM. This uses empirical formulas with forces as a function of the chord position. [29]Shen et al. investigated the ASM on a NACA0015 airfoil. Implementation of a solver of this kind would allow a closer representation to a full rotating geometry CFD model. A full geometry model simulated using direct numerical simulation may be useful for comparison to this and other models, although third party hardware would be needed to make this viable.

In order to improve the validation of complex forms of actuator models, data for full scale offshore turbines is needed. Comparison to large data sets such as LiDAR would further the contributions of this project. In the earlier stages of the project, LiDAR data sets were expected to be received based on the 207MW, 90 turbine Danish wind farm site known as Rødsand 2. Unfortunately the data was not received within the time-span of the project and so the use of experimental data for validation was instead utilised.

This project has mainly focussed on simulation of single turbines using the various actuator models although a second downstream turbine was also introduced. Most industrial applications require modelling of larger arrays of turbines and although the individual models have been evaluated in terms of their viability and suitability for this purpose, their actual performance in this area has not been fully observed. Simulation of large turbine arrays using each model and comparison to large full scale data sets such LiDAR would allow the accuracy of the models in an industrial application to be assessed more completely.

### 5.4.2.   **Suggestions for Model Development**

Based on the use of actuator models throughout the project an issue regard the reliance on input data for each turbine has been identified. The rotational speed or volume force magnitudes must be prescribed for each turbine. These values are dependent on the inflow conditions. For the furthest upstream turbines, they can be easily approximated as the inlet flow conditions are known, but for turbines operating within wakes, the flow conditions entering the turbine swept area are unknown and thus the values are inaccurately chosen. Automatic control of individual turbine parameters based on the characteristics of the incoming flow field would provide great benefit to the models functionality.

# 6. Project Management – Statement of Work

      This Statement of Work (SoW) describes the requirements for the completion of the project. The work to be carried out within the project was well defined to ensure efficient and direct progress towards the overall objectives. A specification of the work required and resulting deliverables was developed in this section as well as a detailed plan for undertaking the project. This SoW was considered a working document and so changes from the initial specifications occurred as the project evolved.

## *6.1.* *Project Scope*

      The project scope included all of the short and long term objectives, work and deliverables of the project. This project was carried out individually but its conclusions were used as part of a group project which had its own more general objectives. These were to improve the practices used to predict the power yield from wind farms. This project looked at the numerical modelling techniques applied to wind turbines in predicting the power yield, specifically those models that use actuator methods to represent the turbines. This involved setting up currently available actuator disk models, which are considered limited in their accuracy and building upon these to develop, analyse and validate more complex models that represented the flow physics more completely. The project therefore required the implementation of a series of increasingly complex models for simulating turbine aerodynamics and wake interaction. The project is limited to actuator models while other modelling techniques are explored as part of concurrent projects that feed into the wider objectives of the group project. Weekly group meetings were carried out to avoid scope creep and ensure progress remained consistent.

## *6.2.* *Work Packages and Deliverables*

      With the models being defined discretely in terms of the techniques they implement, it seemed reasonable to separate the development work into work packages, each relating to a specific model. The following work packages were described in an attempt to break down the project into more manageable sections, each with defined outputs in the form of deliverables. A set of Key Performance Parameters (KPPs) were identified for each deliverable to define their ideal performance. This provided a means to evaluate the success of the project components and identify shortcomings to be improved upon where possible.

| Inputs | Activities | Deliverables | KPPs |
|---|---|---|---|
| **WP-1 Literature Research** | | | |
| Compiled literature from various sources | Summarise relevant theory, procedure, data etc from available literature | Detailed Literature Survey | -Provides a concise summary of main relevant literature to aid in model development |
| **WP-2 Implement Simple Actuator Disk Models** | | | |
| Researched literature on available models i.e. | Implement a range of simple AD models | A range of functional actuator disk models | -Impart volume forces on the flow |

| | | | |
|---|---|---|---|
| Svenning | guided by the literature | | -Induce swirl in the wake. |
| **WP-3 Implement BE Model Coupling** | | | |
| Functional AD model i.e. Svenning model | Modify solver to include blade element method | Functional actuator disk – blade element coupled model | -Produce blade geometry specific simulations. |
| **WP-4 Implement Actuator Line Model** | | | |
| Research Literature on Actuator line models, any pre-existing examples | Develop a solver to implement an actuator line model | Functional actuator line model | -Capable of simulating bound and tip vortices. -Accurately represents specific aerofoil behaviour. |
| **WP-5 Model Analysis and Comparison** | | | |
| Results from simulations of each implemented model | Collect and compare data, preferably power yield prediction | Data and graphical comparisons of the models | -Provide insight into the variations in predictions of different models. |
| **WP-6 Model validation and comparison to experimental/real data** | | | |
| Ouput from WP-5 | Compare model predictions with experimentally obtained data and any other real data available | Data and graphical comparisons of data | -Relate the model predictions to real data in order to evaluate the models effectively against real data. |

## 6.3. Time Management

The time management system that was applied throughout the project involves the use of a Gantt chart to highlight key milestones that represent the time constraints on the project. Subsequently, time periods can be allocated to specific work packages such that progress is kept consistent and deliverables are achieved when needed as a result of the project dependencies. Fig.27 shows the Gantt chart which details the planned and actual time allocation to specific aspects of the project. The chart was amended as the project unfolded.

Fig.27

**Time Management Plan**

| ACTIVITY | PLAN START | PLAN DURATION | ACT. START | ACT. DURATION | % COMPLETE |
|---|---|---|---|---|---|
| **Milestones** | | | | | |
| G1 group Report | 1 | 2 | 1 | 2 | 100% |
| I1 Individual Report | 1 | 9 | 1 | 9 | 100% |
| G2 Group Report | 14 | 16 | 24 | 6 | 100% |
| I2 Individual Report | 14 | 16 | 15 | 15 | 100% |
| Peer Assessments | 29 | 1 | 0 | 0 | 0% |
| Presentation Day | 30 | 4 | 0 | 0 | 0% |
| **Adctuator Disk Project Work** | | | | | |
| WP-1 Literature Review | 2 | 6 | 2 | 6 | 100% |
| WP-2 Implement Simple AD models | 3 | 6 | 4 | 5 | 100% |
| Own pressure-drop model | 3 | 1 | 4 | 1 | 100% |
| Svenning Model | 5 | 4 | 4 | 3 | 100% |
| WP-3 Implement BE method coupling | 12 | 8 | 10 | 9 | 100% |
| Tabulate mexico rotor aerofoil data | 12 | 4 | 16 | 2 | 100% |
| Modify solver to use look-up table | 15 | 5 | 14 | 6 | 100% |
| WP-4 Develop Actuator Line Model | 13 | 11 | 11 | 12 | 100% |
| Study existing AL models | 13 | 6 | 11 | 8 | 100% |
| Modify pisoFoam solver | 15 | 9 | 17 | 8 | 100% |
| WP-5 Model Analyis and Comparison | 14 | 15 | 13 | 15 | 100% |
| Collate data sets from models | 14 | 8 | 15 | 11 | 100% |
| Carry out statistical comparsions | 18 | 9 | 21 | 6 | 100% |
| Review causes of discrepancies | 26 | 1 | 26 | 1 | 100% |
| WP-6 Model validation | 13 | 16 | 11 | 17 | 100% |
| Collate real data (experimental) | 14 | 11 | 14 | 6 | 100% |
| Compare against model outputs | 21 | 7 | 20 | 6 | 100% |
| WP-7 Further Model Development | 23 | 9 | 0 | 0 | 0% |

## 6.4. Risk Assessment

Due to the predominantly theoretical nature of the project, there were very few health and safety risks involved. With large time periods spent sitting at a computer, good posture was always practised and regular breaks were taken to avoid excessive eye strain when using computers for long periods.

There were many risks relating to the success of the project itself. These were identified in the early stages of the project so that they could be mitigated wherever possible and otherwise planned for. The following table summarises the identified project risks and evaluates their relative importance. Actions to prevent, reduce or work around these risks were considered, and as a result the project ran smoothly and free of any major issues.

| Risk | Effect | Cause | Likelihood | Severity | Importance | Action |
|---|---|---|---|---|---|---|
| Compatability issues | Unable to get models operational | Changes to the OpenFOAM definitions between versions. | 10 | 2 | 20 | All models can be adjusted to work on different versions of OpenFOAM given enough time. Ensure time is scheduled for this. |
| Loss of data | Wasted time re-making models etc | File corruption or human error. | 3 | 6 | 18 | Backup all important data in multiple locations |
| Unable to develop functional models | No functional models to analyse. | High level of difficulty in developing certain models. | 1 | 7 | 7 | Make use of pre-existing models available to assess accuracy as a backup and to help develop own models. |
| Unable to obtain experimental data for model validation | No tool for validation of models. | Failure to deliver by the experimental team. | 2 | 5 | 10 | Compile data from pre-existing sources to use as a backup tool for validation |
| Meshing Time and CFD Run time | May not receive model results in time for detailed analysis | Complex cases have a high computational expense. Limited resources are available | 5 | 5 | 25 | Run simplified cases first to analyse time demand for high fidelity cases. Use of external hardware i.e. cfms cluster allows reduced run times via parallel run. |
| Group Demands | Other members of the group may require assistance. | High level of difficulty in other areas of the group project i.e LES ABL solvers etc. | 3 | 3 | 9 | Regular group meetings allow time schedule adjustment to be made ahead of time |

## 6.5. Wider Social, Environmental and Economic Implications of the Project

Due to the strong environmental benefit of renewable energy usage, this project has a heavy bearing on future developments in clean energy generation. As of yet wind power has not been capitalized on to the extent possible. This is largely the result of a lack of commercial investment in wind power. Availability of improved methods for power yield prediction causes

a more predictable return on any commercial investment. This may improve the appeal of wind power as a lower risk investment opportunity thereby increasing the global scale of the wind power generation industry. The ability to compare the relative accuracies and costs of different modelling techniques will also allow existing wind energy companies to more effectively model proposed wind farm sites and improve the resulting wind farm design to maximise power yield.

# 7. Contribution to Group Functioning

## 7.1.    Technical Contributions

The investigation presented in this report formed part of a larger investigation with well defined overall objectives. The conclusions of this investigation allowed one of the major existing forms of turbine models to be evaluated and its potential for becoming an improved commercial technique analysed. The main group objective largely relied on identification of the reasons why current techniques are not able to predict turbine power yield at an acceptable level of accuracy. Since actuator models are one of the most common current models for wind turbines, a full analysis of this model variety contributes to the group aims. This investigation, along with accompanying external factor investigations such as atmospheric boundary layer simulation and wind angle analysis, plus development of improved model functionality such as automatic turbine rotor speed adjustment and free spinning functionality, explored within the group represents important first steps in improving the current situation of turbine modelling and power predictive methods.

## 7.2.    Group Dynamics and Management

Weekly meetings were held during term times to report on progress and allow group problem solving. The roles of meeting chairmen, responsible for preparing the meeting agenda and conducting the meeting, and secretary, responsible for recording and sharing the meeting minutes were rotated on a weekly basis. This allowed all members of the group to share the responsibilities and contribute to the group functioning.

A considerable amount of time was also spent aiding other members of the group on solving issues that they experienced, mostly with regard to debugging of CFD model implementations but also with evolution of project directions to align with the group objectives. In this manner an important contribution has been made to the investigations of other individuals within the group project.

# References

1 Froude RE. (1889) *On the part played in propulsion by difference in pressure*. Transaction of the Institute of Naval Architects, 30: 390–423.

2 Rankine, WJM. (1865) *On the mechnical principles of the action of propellers*. Transaction of the Institute of Naval Architects, 6: 13–39.

3 Betz A. (1920) Das *maximum der theoretisch möglichen ausnützung des windes durch windmotoren.* Zeitschrift für das gesamte Turbinewessen, 307–309.

4 Glauert H. (1963) *Airplane propellers.* Aerodynamic Theory. Dover, New York, 169-269

5 Wu TY. (1962) *Flow through a heavily loaded actuator disc*. Schifftechnik, 9: 134–138.

6 Hough GR, Ordway DE. (1965) *The generalized actuator disc*. Developments in Theoretical and Applied Mechanics, Pergamon Press, Oxford,; 2: 317–336.

7 Greenberg MD. (1972) *Nonlinear actuator disc theory*. Zeitschrift fu¨r Flugwissenschaften, 20(3): 90–98.

8 Conway JT. (1995) *Analytical solutions for the actuator disc with variable radial distribution of load*. J. Fluid Mech., 297: 327–355.

9 Sørensen JN, Myken A. (1992) *Unsteady actuator disc model for horizontal axis wind turbine*. J. Wind Eng. Ind. Aerodyn.,; 39: 139–149.

10 Sørensen JN, Kock CW. (1995) *A model for unsteady rotor aerodynamics*. J. Wind Eng. Ind. Aerodyn. 58: 259–275.

11 Sørensen JN, Shen WZ, Munduate X. (1998) *Analysis of wake states by a full-field actuator disc model*. Wind Energy, 1: 73–88.

12 Madsen HA. (1996) *A CFD analysis of the actuator disc flow compared with momentum theory results*. Proc. 10th IEA Symp. on the Aerodynamics of Wind Turbines, Edinburgh, 109–124.

13 Masson C, Smaïli A, Leclerc C. (2001) *Aerodynamic analysis of HAWTs operating in unsteady conditions*. Wind Energy, 4: 1–22.

14 A. Javaheri, B. Cañadillas (2013) *Wake Modeling of an Offshore Wind Farm Using OpenFOAM*; DEWI GmbH, Wilhelmshaven

15 Svenning, E. (2010) *Implementation of an actuator disk in OpenFOAM*. CFD with open-source software. Chalmers University of Technology.

16 Mikkelsen R, Sørensen JN, Shen WZ. (2001) *Modelling and analysis of the flow field around coned rotors*. Wind Energy, 4: 121–135.

17 Jeromin, A. Bentamy, A. and Schaffarczyk A. P. (2014) *Actuator disk modelling of the Mexicorotor with OpenFOAM*. ITM Web of Conferences. 2014, 2: 1-12.

18 Sørensen JN, Shen WZ. (2002) Numerical modeling of wind turbine wakes. J. Fluids Engineering, ASME Trans. 124: 393–399.

19 Fleming P. P. Fleming, S. Lee, M. Churchfield, A. Scholbrock, J. Michalakes, K. Johnson, and P. Moriarty (2013) *The SOWFA Super-Controller: A High-Fidelity Tool for Evaluating Wind Plant Control Approaches.* National Renewable Energy Laboratory

20 Gebreslassie, M., Tabor, G., Belmont, M. (2015) *Investigation of the Performance of a Staggered Configuration of Tidal Turbines Using CFD,* College of Engineering, Mathematics and Physical Sciences, University of Exeter.

21 J. Jonkman, S. Butterfield, W. Musial, and G. Scott, (2009) *Definition of a 5-MW Reference Wind Turbine for Offshore System Development*, National Renewable Energy Laboratory.

22 J.G. Schepers H. Snel, *Model Experiments in Controlled Conditions*, Energy Research Centre of the Netherlnds, 2007

23 Goldstein S. (1929) *On the vortex theory of screw propellers*. Proc. Royal Soc; 123 A: 440–465.

24 N. Troldborg. (2008) *Actuator Line Modeling of Wind Turbine Wakes*. PhD thesis, Technical University of Denmark, Lyngby, Denmark.

25 H. Versteeg, W. Malalasekera, (2007) *An Introduction to Computational Fluid Dynamics*, 2nd Edition, Pearson Education Limited, Harlow, England.

26 Kolmogorov A. N. (1991) *The local structure of turbulence in incompressible viscous fluid for very large Reynolds numbers*. Dokl. Akad. Nauk., Vol. 30, pp. 301 – 305, 1941. Reprinted Proc. Royal Soc. London; 434; 9; 1991.

27 Villiers, E. The *Potential of Large Eddy Simulation for the Modeling of Wall Bounded Flows*, Department of Mechanical Engineering Imperial College of Science, Technology and Medicine p59-69 (2006)

28 V´aclav Kol´aˇr, (2007) *Vortex identification: New requirements and limitations International Journal of Heat and Fluid flow* 638-652

29 W.Z. Shen, J.H. Zhang, and J.N. Sørensen. (2009) The *actuator surface model: A new navier–stokes based model for rotor computations.* Journal of Solar Energy Engineering, 131(1):011002.